Palaeogeography, Palaeoclimatology, Palaeoecology 401 (2014) 81–95

Contents lists available at ScienceDirect

Palaeogeography, Palaeoclimatology, Palaeoecology

journal homepage: www.elsevier.com/locate/palaeo

Late Miocene to early Pliocene climate variability off NW Africa (ODP Site 659)

Christophe Colin [a,*], Giuseppe Siani [a], Zhifei Liu [b], Dominique Blamart [c], Charlotte Skonieczny [d], Yulong Zhao [b], Aloys Bory [d], Norbert Frank [e], Stéphanie Duchamp-Alphonse [a], François Thil [c], Thomas Richter [f], Catherine Kissel [c], Julien Gargani [a]

[a] IDES — Laboratoire des Interactions et Dynamique des Environnements de Surface (UMR 8148), Département des Sciences de la Terre Université Paris-Sud XI, 91405 Orsay, France
[b] State Key Laboratory of Marine Geology, Tongji University, Shanghai 200092, China
[c] LSCE — Laboratoire des Sciences du Climat et de l'Environnement (UMR 1572 CEA-CNRS-UVSQ), Domaine du CNRS, Avenue de la Terrasse, F-91118 Gif sur Yvette, France
[d] GEOSYSTEMES (FRE CNRS 3298), Université de Lille I, 59655 Villeneuve d'Ascq, France
[e] Institut für Umweltphysik, Physik der Umweltarchive, Universität Heidelbergnsérer numérotationligne, Im Neuenheimerfeld 229, 69120 Heidelberg, Germany
[f] Royal Netherlands Institute for Sea Research, P.O. Box 59, 1790 AB Den Burg, Netherlands

ARTICLE INFO

Article history:
Received 9 October 2013
Received in revised form 7 February 2014
Accepted 9 February 2014
Available online 18 February 2014

Keywords:
African monsoon
ITCZ
Dust input
Messinian Salinity Crisis
Cape Verde plateau

ABSTRACT

A high resolution $\delta^{18}O$ record obtained on benthic foraminifera (*Cibicides wuellerstorfi*) combined with clay mineralogy, major element concentrations and Sr–Nd isotopes have been investigated for the ODP Site 659 located off North Africa in order to reconstruct African monsoon intensity between 6.2 and 4.9 Myr. Mineralogical and geochemical results indicate that sedimentation on the Cape Verde plateau results from a mixture of sediments deriving from the neighbouring Saharan arid region and the wet African equatorial zone (Sahelian Band), characterised by a low and a high state of weathering, respectively. Past variations in terrigenous inputs from these areas allow us to track past extension and displacement of the West African Monsoon–ITCZ system. Maximal summer insolation induced a northward migration of the inter-tropical convergence zone (ITCZ), wetter conditions in the Sahel, and a diminishing of wind erosion over the South Sahara and Sahel. In addition, there was an increase in river input to the Cape Verde plateau of sediments derived from southern sedimentary sources, which are characterised by high kaolinite contents and CIA values and low K/Al and Ti/Al ratios. On the other hand, minimal summer insolation induced a southward movement of the ITCZ, drier climate in the Sahel and stronger easterly winds resulting in an increase in dust transport from the Sahara to the Cape Verde Plateau. Dust particles are characterised by high illite and smectite content and by a low chemical state of weathering (low CIA values and high K/Al and Ti/Al ratios). Finally, our results provide new clues regarding the re-flooding of the Mediterranean Sea at the end of the MSC (5.33 Myr). This event was associated with enhanced aridity in the Sahara, implying a reorganisation of the atmospheric circulation and a southward migration of the ITCZ.

1. Introduction

The northern part of Africa is affected by a climatic system of monsoon type, characterised by a latitudinal subdivision of climatic zones between the Saharan arid region and the wet Sahelian zone. This is a consequence of the seasonal migration of the intertropical convergence zone (ITCZ) controlled by variations in the insolation received by the African continent. Today, the ITCZ is centred at about 20°N during the boreal summer and generates a wet climate on the Sahel and easterly winds that favour Saharan dust input to the North Equatorial Atlantic between latitudes of 10 and 30°N (Fig. 1) (Ruddiman et al., 1986; Swap et al., 1996). During the boreal winter, the ITCZ migrates southward to a latitude of around 0–5°N inducing a dry climate in the Sahel and Sahara regions. At that time of the year, dust is carried by middle altitude winds over the tropical Atlantic between 10°N and 5°S (Fig. 1) (Prospero and Carlson, 1981; Ruddiman et al., 1986). In the past, migrations of the ITCZ have been mainly controlled by the atmospheric pressure gradient between the Atlantic Ocean and Africa. This was mainly a result of variations in the insolation received by the earth at low latitudes (Tiedemann et al., 1994) and in sea surface temperature in the Gulf of Guinea. During the Plio-Pleistocene, North African monsoon intensity oscillated from humid to arid periods following periodicities of the precession (19 and 23 kyr) (Tiedemann et al., 1994) and to a lesser extent by glacial–interglacial cyclicities (deMenocal et al., 1993; deMenocal, 1995a,b; Tuenter et al., 2003).

Recent studies have shown that clay mineralogical composition can provide information on the provenance of mineral dusts originating

* Corresponding author. Tel.: +33 1 69 15 67 85; fax: +33 1 69 15 48 82.
E-mail address: christophe.colin@u-psud.fr (C. Colin).

http://dx.doi.org/10.1016/j.palaeo.2014.02.015
0031-0182/

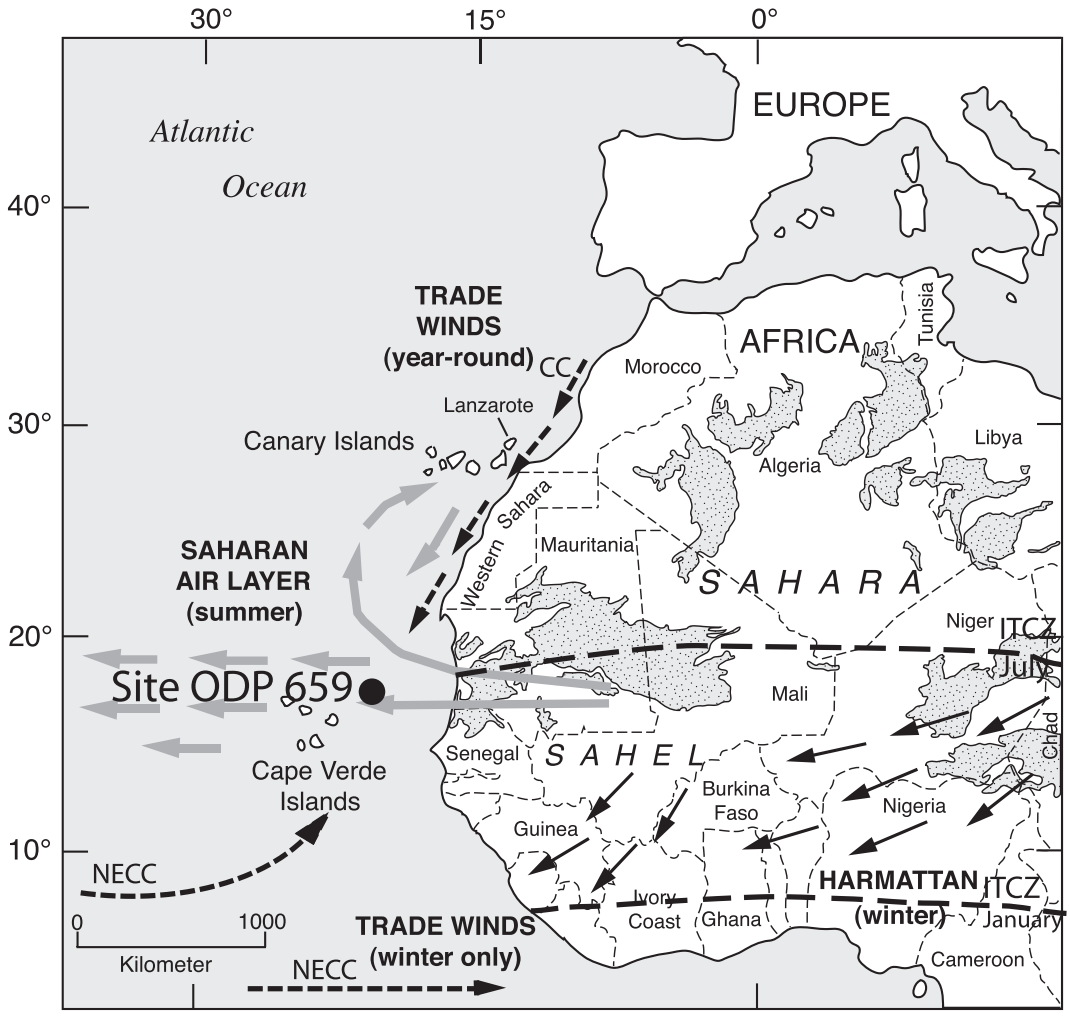

Fig. 1. Map showing north-western Africa, the location of the ODP Site 659, localities referred to in the text, the surface sea currents, the main dust-transporting winds and their seasons of transport. Also shown (grey stippled areas) major active sand. NECC: North Equatorial Counter Current. CC: Canary current.

from North Africa (e.g. Caquineau et al., 1998; Formenti et al., 2011; Skonieczny et al., 2011; Scheuvens et al., 2013; Skonieczny et al., 2013). Indeed, distributions of kaolinite and illite in northwestern Africa are highly dependent on the efficiency of weathering processes in soils and present a latitudinal distribution (Paquet et al., 1984). Illite is present in high proportions in dust deriving from the Sahara whereas kaolinite is abundant in Sahelian and tropical African soils (Pastouret et al., 1978; Paquet et al., 1984). Consequently, the illite/kaolinite ratio decreases markedly from north to south throughout the Saharan/Sahelian latitudinal band and can be used to track the provenance of the eolian dust input to the Northeastern Tropical Atlantic Ocean (NETAO) (Caquineau et al., 1998; Scheuvens et al., 2013; Skonieczny et al., 2013).

The sediments of the Ocean Drilling Program (ODP) at Site 659 collected off the East African shelves constitute an ideal archive to reconstruct past changes in the North-African monsoon (Ruddiman and Janecek, 1989; Tiedemann et al., 1994) as they provide a record of the African terrigenous material supplying the NETAO and, more particularly, the eolian inputs controlled by aridity conditions in North Africa (Prospero and Nees, 1986; deMenocal et al., 1993; deMenocal, 1995a,b) (Fig. 1).

This paper reports on a high-resolution study of sedimentology, clay mineralogy, major and trace elements and Sr–Nd isotopic data from the ODP Site 659. The study has been carried out in order to reconstruct the paleoenvironmental changes that affected North Africa between 6.2 and 4.9 Myr through: (1) the identification of the sediment source(s) supplying the NETAO; (2) the identification of the sediment transport pathways to the Cap Verde plateau and (3) the establishment of possible links between African monsoon variability and the paleoenvironmental changes associated with the Messinian Salinity Crisis (MSC) in the Mediterranean Sea. The MSC is characterised by the deposition of a large volume of evaporites (1500 m, Clauzon, 1982) in the Mediterranean basin (Hsü et al., 1973) and it has been dated to between 5.96 and 5.33 Ma (Gautier et al., 1994; Krijgsman et al., 1999a). This event is associated with major paleo-environmental changes including a huge sea-level fall in the Mediterranean Sea (at least 1500 m) that could have had an impact on the climate of North Africa, a hypothesis which has been never tested (Murphy et al., 2009; Schneck et al., 2010). The establishment of a high resolution tuning orbital age scale, combined with a high-resolution benthic foraminifera $\delta^{18}O$ record and biostratigraphic data have been already reported by Colin et al. (2008) which allows here new comparison between mineralogical and geochemical record of the ODP Site 659 and events which occurred during the late Miocene in the Mediterranean Sea. The potential links between precipitation changes in north-eastern Africa and variations of the African monsoon and other climatic processes, such as the MSC in the Mediterranean Sea, are discussed.

2. Materials and methods

The ODP Site 659 (Leg 108) is located on the Cap Verde plateau approximately 350 km off the coast of Mauritania (18°04′63″N, 21°01′57″W; 3071.2 m water depth) (Fig. 1). The studied sedimentary unit

consists of lithological homogeneous hemipelagic ooze corresponding to the depth interval between 146 and 167 mcd (meter composite depth). No turbidite layers were observed in the studied sedimentary sequence.

A total of 300 samples, collected at constant sampling intervals, were selected for calcareous nannofossil biostratigraphic analysis. Smear slides were prepared using the method of Watkins and Bergen (2003) and were then examined under a cross-polarized transmitted light microscope. The first occurrence (FO), last occurrence (LO) and first consistent occurrence (FCO) of species are used to define ODP Site 659 nannofossil datum levels, which are then related to the calcareous nannofossil biostratigraphic events reported by Raffi et al. (2006).

$\delta^{18}O$ values, expressed in ‰ versus VPDB (Vienna Pee Dee Belemnite standard) were determined on the benthic foraminifera *Cibicides wuellerstorfi*. Six to ten shells were picked in the 250–315 μm size range. Prior to isotopic analyses, the samples were cleaned in a methanol ultrasonic bath for a few seconds and then roasted under vacuum at 380 °C for 45 min. Isotopic analyses were performed at LSCE on Finnigan Delta + mass-spectrometers. VPDB is defined with respect to NBS19 calcite standard (Coplen et al., 1983). The mean external reproducibility (1σ) of carbonate standards is ±0.05‰, measured NBS18 $\delta^{18}O$ is −23.2 ± 0.2‰ VPDB.

Carbonate contents have been analyzed every 5 cm (547 samples) using the gasometric techniques of Jones and Kaiteris (1983) with a precision better than ±2% at the Laboratoire IDES (University of Paris XI). Volume low field magnetic susceptibility (k) has been obtained using u-channel samples (Weeks et al., 1993) at LSCE. The measurements have been done using a Bartington MS2C 45-mm diameter susceptibility bridge at 2 cm intervals with a resolution of about 4 cm.

A total of 323 samples were taken at 5 to 10 cm intervals throughout Site 659 in order to perform clay mineralogy analyses. Clay minerals were identified by X-ray diffraction (XRD) using a PANalytical diffractometer at the Laboratoire IDES on oriented mounts of non-calcareous clay-sized (<2 μm) particles. The oriented mounts were obtained following the methods described in detail by Liu et al. (2004). Three XRD runs were performed, following air-drying, ethylene-glycol solvation for 24 h, and heating at 490 ºC for 2 h. Identification of clay minerals was carried out primarily according to the position of the (001) series of basal reflections on the three XRD diagrams. Semi-quantitative estimates of peak areas of the basal reflections for the main clay mineral groups of smectite (including mixed-layers) (15–17 Å), illite (10 Å), and kaolinite/chlorite (7 Å) were carried out on the glycolated curve (Fig. 2) using the MacDiff software (Petschick, 2000). Mixed-layers composed mainly of smectite–illite (15–16 Å) are included in the "smectite" category. Relative proportions of kaolinite and chlorite were determined based on the ratio from the 3.57/3.54 Å peak areas. Replicate analyses of a few selected samples gave a precision of ±2% (2σ). Based upon the XRD method, the semi-quantitative evaluation of each clay mineral has an accuracy of ~4%. Additionally, illite crystallinity was obtained from half height width of the 10 Å peak on the glycolated curve. Lower values represent higher crystallinity, characteristic of weak hydrolysis in continental sources and cold, arid climate conditions (Chamley, 1989).

Detrital XRF geochemical data were obtained directly on the surfaces of split cores at 1 cm resolution, using the Avaatech XRF core-scanner at the Royal Netherland Institute for Sea Research (NIOZ) (Richter et al., 2006). The measurements were performed at 10 kV and 500 mA to obtain intensities for several major elements (aluminium (Al), silicon (Si), potassium (K) and titanium (Ti)).

Analysis of geochemical composition, including major elements, Sr and Nd concentrations and Sr–Nd isotopes, was performed on the carbonate free-fraction of samples. Samples were de-carbonated by leaching with a 20% acetic acid solution in an ultrasonic bath, then rinsed five times and centrifuged to eliminate the carbonate solution. Major element content analyses were performed on 140 samples measured by inductively coupled plasma optical emission spectrometry (ICP-OES) using an IRIS Advantage instrument at the State Key Laboratory of Marine Geology, Tongji University. About 30–40 mg of oven-dried sediments were heated at 600 °C to achieve the loss of ignition (LOI). The sample was then dissolved using a mixed solution of HNO_3 + HF on a hot plate. The eluted sample was diluted 1000 times with 2% HNO_3 for the major-element measurement. Replicate analyses of GSR-5, GSR-6, and GSD-9 reference samples during the study gave an accuracy of 4% for major elements. Replicate analyses of selected samples gave a precision of ±2% (2σ).

The $^{143}Nd/^{144}Nd$ ratio was determined using static multicollection on a Finnigan MAT-262 and the $^{87}Sr/^{86}Sr$ ratio was analyzed using a Finnigan Neptune-Plus Multi-collector Inductively Coupled Plasma Mass Spectrometry (MC-ICP-MS) at the Laboratoire des Sciences du Climat et de l'Environnement (LSCE, Gif/Yvette). Following the procedure described by Colin et al. (1999), samples were dissolved in HF-$HClO_4$ and HNO_3–HCl mixtures. The first chemical separation utilised Biorad columns packed with AG50WX-8, 200–400 mesh cation exchange resin. Sr and Rb were then eluted with 2 N HCl and the light rare-earth elements with 2.5 N HNO_3. The Sr fraction was purified on a 20 μl SrSpec® column consisting of a polyethylene syringe with a 4 mm ∅ Millex® filter. Nd was isolated by reverse-phase chromatography on HDEHP-coated Teflon powder. $^{87}Sr/^{86}Sr$ ratios were corrected for mass fractionation using normalisation to a $^{86}Sr/^{88}Sr$ ratio = 0.1194. Replicate analyses of NIST SRM987 (n = 20) during the study gave a mean $^{87}Sr/^{86}Sr$ of 0.710263 ± 0.000016 (2σ). This mean value is close to its certified value of 0.710250, suggesting a negligible (0.000013) machine bias that was taken into consideration. Similarly, $^{143}Nd/^{144}Nd$ ratio was corrected for mass fractionation using a normalisation to the natural $^{146}Nd/^{144}Nd$ ratio = 0.7219. Replicate analyses (n = 10) of the LaJolla standard gave a mean $^{143}Nd/^{144}Nd$ of 0.511853 ± 0.000007, close to its certified value of 0.511860. For convenience, Nd isotopic ratio results are expressed as $\varepsilon Nd(0) = [(^{143}Nd/^{144}Nd_{meas})/0.512638) - 1] \times 10{,}000$, using the CHUR value given by *Jacobsen and Wasserburg* [1980]. Sr and Nd concentrations were analyzed by inductively coupled plasma-mass spectrometry (ICP-MS) using a Thermo VG-X7 mass spectrometer at the State Key Laboratory of Marine Geology, Tongji University. About 30–40 mg of pre-prepared sediments were heated in an oven at 600 °C. The sediments were then dissolved on a hot plate using a mixed solution of HNO_3 + HF. The eluted sample was diluted using 2% HNO_3 for the Sr and Nd measurement. Uncertainties for concentration measurement for Sr and Nd are <3%.

3. Chronological framework

Results of the calcareous nannoplancton investigation for the studied interval of Site 659 indicate 3 bio-events: i) the last occurrence of *Amaurolithus amplificus* (163.72 mcd) dated at 5.993 ± 0.002 Myr; ii) the last occurrence of *Discoaster quinqueramus* (152.74 mcd), dated at 5.537 ± 0.005 Myr (Backman and Raffi, 1997) and iii) the first occurrence of *Ceratolithus acutus*, (148.76 mcd) dated at 5.372 ± 0.003 Myr (Backman and Raffi, 1997; Colin et al., 2008) (Fig. 2). In addition, oxygen isotope analyses ($\delta^{18}O$) were performed on the benthic foraminifera *C. wuellestorfi* (Fig. 2). $\delta^{18}O$ variations range from 2.7 to 3.6‰ (PDB) showing similar climatic variability in the late Neogene characterised by several maxima (minima) of the $\delta^{18}O$ values indicating glacial (interglacial) stages (Shackleton et al., 1995). The excursions of the highest isotopic values correspond to the major glacial stages TG22 and TG12 dated respectively at 5.84 and 5.55 Myr. This is in agreement with the results of the previous studies (Shackleton et al., 1995; Shackleton and Crowhurst, 1997; Hodell et al., 2001), thus providing further temporal constraints.

The age model of the ODP Site 659 was initially established by a linear interpolation between the occurrence of the three inferred bio-events and the identification of TG12 and TG22 revealed by the $\delta^{18}O$ record (Fig. 2). To establish an orbital age model, the $\delta^{18}O$ record of

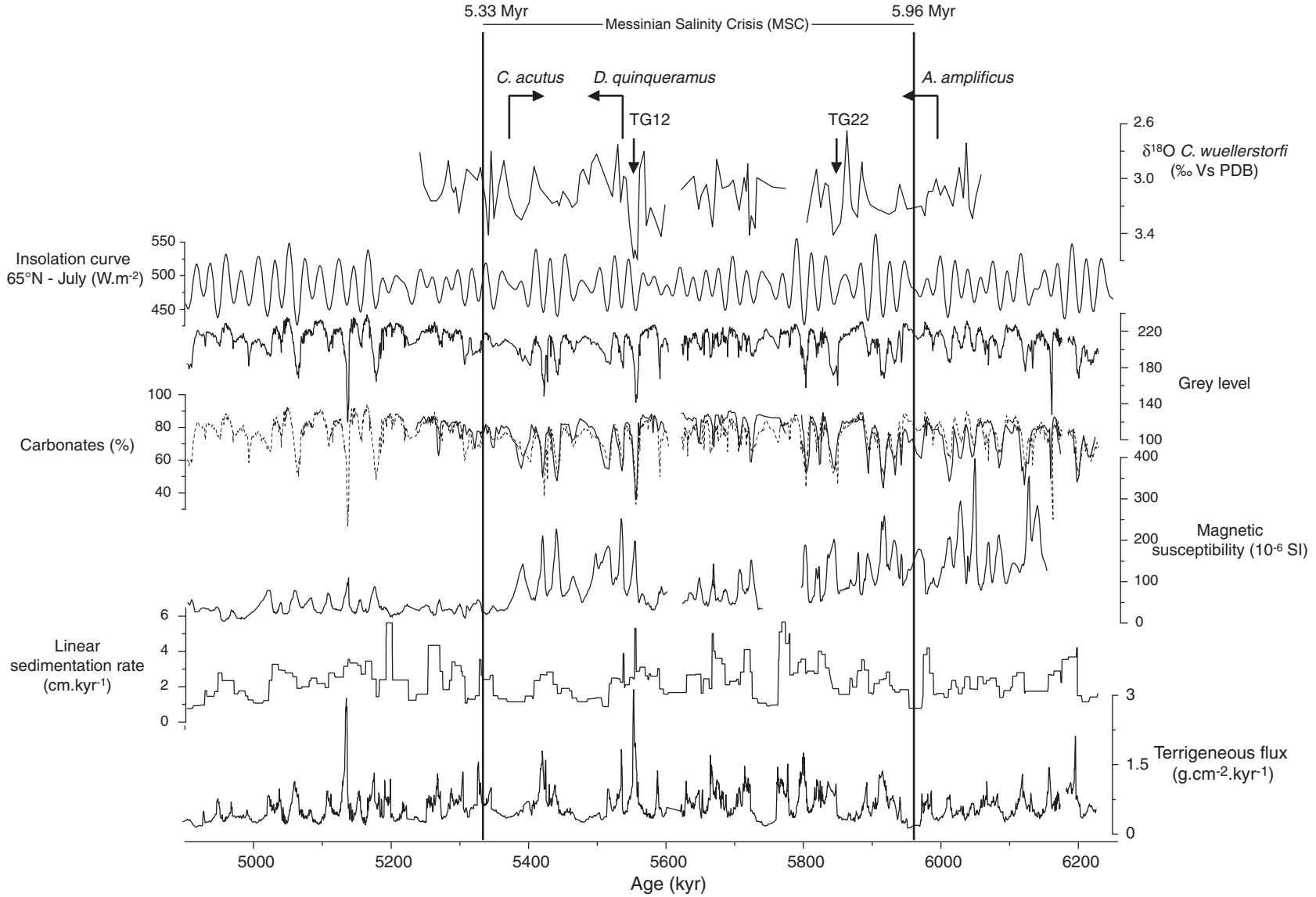

Fig. 2. Variations of *C. wuellerstorfi* $\delta^{18}O$ (‰), grey level, carbonate contents (% wt), low field susceptibility (10^{-6} SI) and linear sedimentation rates (cm.kyr^{-1}) versus age (kyr). The dotted line represents variations in the carbonate contents estimated from the grey level. Time points from the biostratigraphical investigation are also displayed. Insolation curve (W.m^{-2}) calculated for the month of July at latitude of 65°N using the Analyserie software (Paillard et al., 1996) is also reported for comparison. Terrigeneous fluxes were calculated using the following relationship: $Flux_{tot} = \rho_s.Tx$ and $Flux_{tot} = (100 - C).Flux_{det} + C.Flux_{car}$ where, $Flux_{tot}$, $Flux_{det}$ and $Flux_{Car}$ correspond to total, terrigeneous and carbonate fluxes (g.cm^{-2}.ka^{-1}), respectively; C = biogenic carbonate proportion (%); ρs = dry bulk density (g.cm^{-3}) and Tx = linear sedimentation rate (cm.ka^{-1}).

C. wuellerstorfi was combined with low field magnetic susceptibility (χ) and grey level measurements (Colin et al., 2008). χ varies between 40 and 400 $*$ 10^{-6} SI with higher amplitudes of variations before 5.4 Myr (Fig. 2). The grey level is inversely correlated to magnetic susceptibility and ranges from 120 to 230 (Fig. 2). Blackman–Tukey spectral analyses performed using the Analyseries software (Paillard et al., 1996) on the magnetic susceptibility, grey levels and $\delta^{18}O$ records indicate periodicities close to those of the orbital parameters of obliquity and precession (Colin et al., 2008). In order to provide a robust chronological framework, a two-step tuning was performed on the $\delta^{18}O$ filtering signal with obliquity and on a 23 kyr magnetic susceptibility and grey level filtering with the insolation curve calculated for 65°N latitude in July (Tiedemann et al., 1994; Laskar et al., 2004).

According to the age model, the ODP Site 659 provides a continuous record between 6.2 and 4.9 Myr (Fig. 2), with an average linear sedimentation rate (LSR) of about 2.6 cm/kyr. The LSR was highly variable between 0.7 and 5.7 cm/kyr. The highest (5.7 cm/kyr) and lowest (0.7 cm/kyr) LSR values are observed at around 5.77 Myr and 4.90 Myr respectively. The inferred LSR estimates permit us to obtain a mean time resolution of 4 kyr and 0.52 kyr for clay mineralogical and XRF geochemical data respectively.

4. Results

4.1. Carbonate contents and terrigenous fluxes

Biogenic carbonate content ranges between 30 and 90% wt and fits well with the grey level variations (Fig. 2). Microscope observation combined with XR diffraction analyses of the ODP Site 659 sediments indicate a carbonate fraction dominated by planktonic foraminifera and coccoliths without detritic carbonate (dolomite). Terrigenous fluxes were calculated in order to assess detrital input to the Cap Verde plateau without any influence of the carbonate dilution and compaction of sediment. The terrigenous flux record varies significantly between 0.14 and 2.13 $g.cm^{-2}.kyr^{-1}$ with an average value of 0.65 $g.cm^{-2}.kyr^{-1}$ (Fig. 2). Such average value is similar to those calculated by Tiedemann et al. (1994) and Stein and Sarnthein (1984) prior to 5 Myr (0.70 $g.cm^{-2}.kyr^{-1}$) on the NETAO and is two time lower than the average terrigenous flux of the late Quaternary (1.25 $g.cm^{-2}.kyr^{-1}$ for the last 400 kyr) calculated from the ODP Site 659 (Tiedemann et al., 1994). The terrigenous flux correlates well with the insolation curve calculated for 20°N in July (Fig. 4). In general, minima of summer insolation correspond to an increase in terrigenous fluxes (up to 1.2 $g.cm^{-2}.kyr^{-1}$) implying that the sedimentation of the ODP Site 659 was controlled by changes in the intensity of the African monsoon.

4.2. Clay mineralogy

The clay mineral assemblage of ODP Site 659 sediments is composed of smectite, kaolinite, illite, chlorite and palygorskite (Fig. 3). In general, smectite, illite–palygorskite and kaolinite distributions reveal distinct temporal evolution. Long-term changes in smectite content are inversely correlated to those of kaolinite. Smectite contents (average 35%) display the largest variations, ranging from 20 to 62%. Prior to ~5.3 Myr, smectite content varies between 20% and 54% with an average value of 33% whereas thereafter it varies between 30% and 62% (average 41%). Kaolinite is the predominant mineral (average value ~ 39%) and

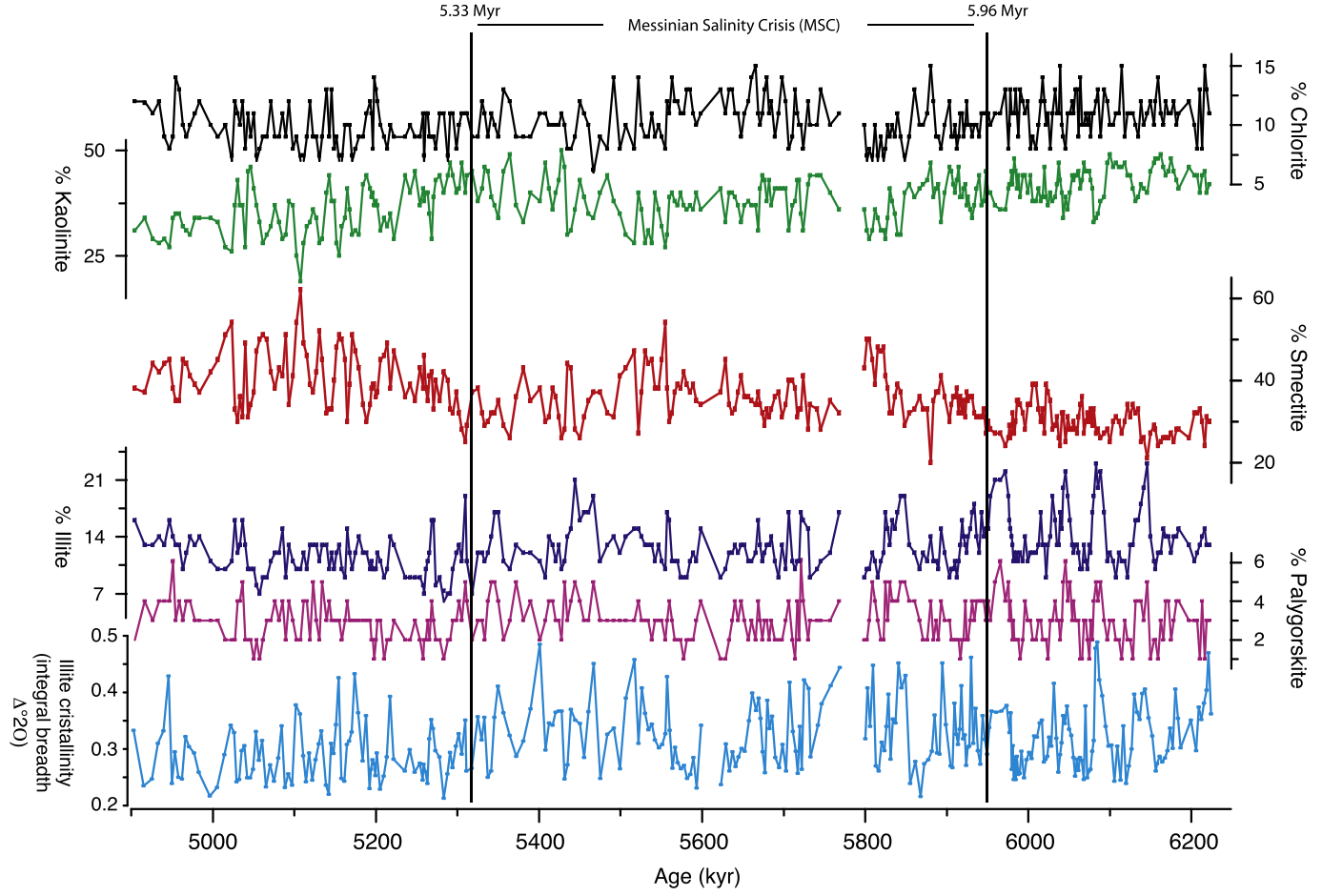

Fig. 3. Variations in clay mineral proportions (%) on the <2 μm size fraction and illite cristallinity values (integral breadth Δ°2Theta) versus age (kyr) for ODP Site 659.

displays variations ranging from 25% to 50%. Long-trend changes are also well-marked in kaolinite contents with a significant decrease from 49 to 25% between 5.3 and 4.9 Myr.

The illite content varies between 6 and 23% (average value ~ 13%) (Fig. 3). The highest values were recorded before ~ 5.3 Myr, (average value ~ 15%), whereas thereafter it decreases reaching a mean value of ~11%. The proportion of palygorskite is extremely low (~1–6%) but its distribution is correlated with that of illite. At a shorter time scale, each increase of the illite–palygoskite proportion is associated with a decrease in the kaolinite content. Chlorite contents range from 6% to 15%, with no long-term variations observed.

As chlorite and palygorskite do not present major variations in Site 659, the smectite/kaolinite and the illite/kaolinite ratios have been used to describe the mineralogical changes within the clay fraction (Fig. 4). Smectite/kaolinite and the illite/kaolinite ratios present large variations between 0.42 to 3.25 and 0.14 to 0.67, respectively (Fig. 4). Changes in smectite/kaolinite and illite/kaolinite ratios show similar precession-related (23 kyr) oscillations correlating the mineralogical characteristics with the solar radiation calculated at 20°N for July (Fig. 4). In general, the insolation curve minima are correlated with an increase of both mineralogical ratios. At a longer time scale, the smectite/kaolinite ratio, and to a lesser extent illite/kaolinite ratio, increase significantly after 5.3 Myr.

In addition, illite crystallinity varies significantly between 0.21 and 0.42 and is also correlated with the insolation curve. In general each minimum of the summer insolation curve is associated with an increase of the illite crystallinity values.

4.3. Major and trace elements

The elements of Si, K and Ti, which are representative of elements derived from detrital inputs, are reported herein to investigate the geochemical changes in terrigenous sediments. Owing to its conservative behaviour in weathering profiles, Al is employed as a normalising parameter to assess relative degrees of enrichment/depletion of specific elements and to eliminate dilution from carbonate and organic fractions (Calvert and Pedersen, 2007). Therefore, Si/Al, K/Al and Ti/Al ratios, obtained every 1 cm by using the Avaatech XRF core-scanner, have been reported in Fig. 5. The X-ray fluorescence (XRF) core scanner provides bulk-sediment chemistry data measured non-destructively at the split core sediment surface. Although this method is widely accepted, little is known about the effects of physical properties such as density, matrix effects and water content on XRF core scanner data. Recent studies indicate that the water film developed between the sediment surface and the Ultralene® foil, as well as the interstitial water near the sediment surface, have a considerable influence on the XRF intensities of the lighter elements Al and Si (Kido et al., 2006). In contrast, the heavier elements K, Ti, and Fe remain relatively unaffected by variations in physical properties (Tjallingii et al., 2007). Consequently, to determine any potential problems stemming from the effects of physical properties on the geochemical ratios, we have also reported in Fig. 5 similar ratios of major element contents on the carbonate-free fraction by ICP-OES analyses. Variations in Si/Al, K/Al and Ti/Al obtained by both methods are well correlated ($r = 0.79$ for Si/Al; $r = 0.66$ for K/Al; $r = 0.56$ for Ti/Al) confirming that the XRF core-scanner results are not strongly

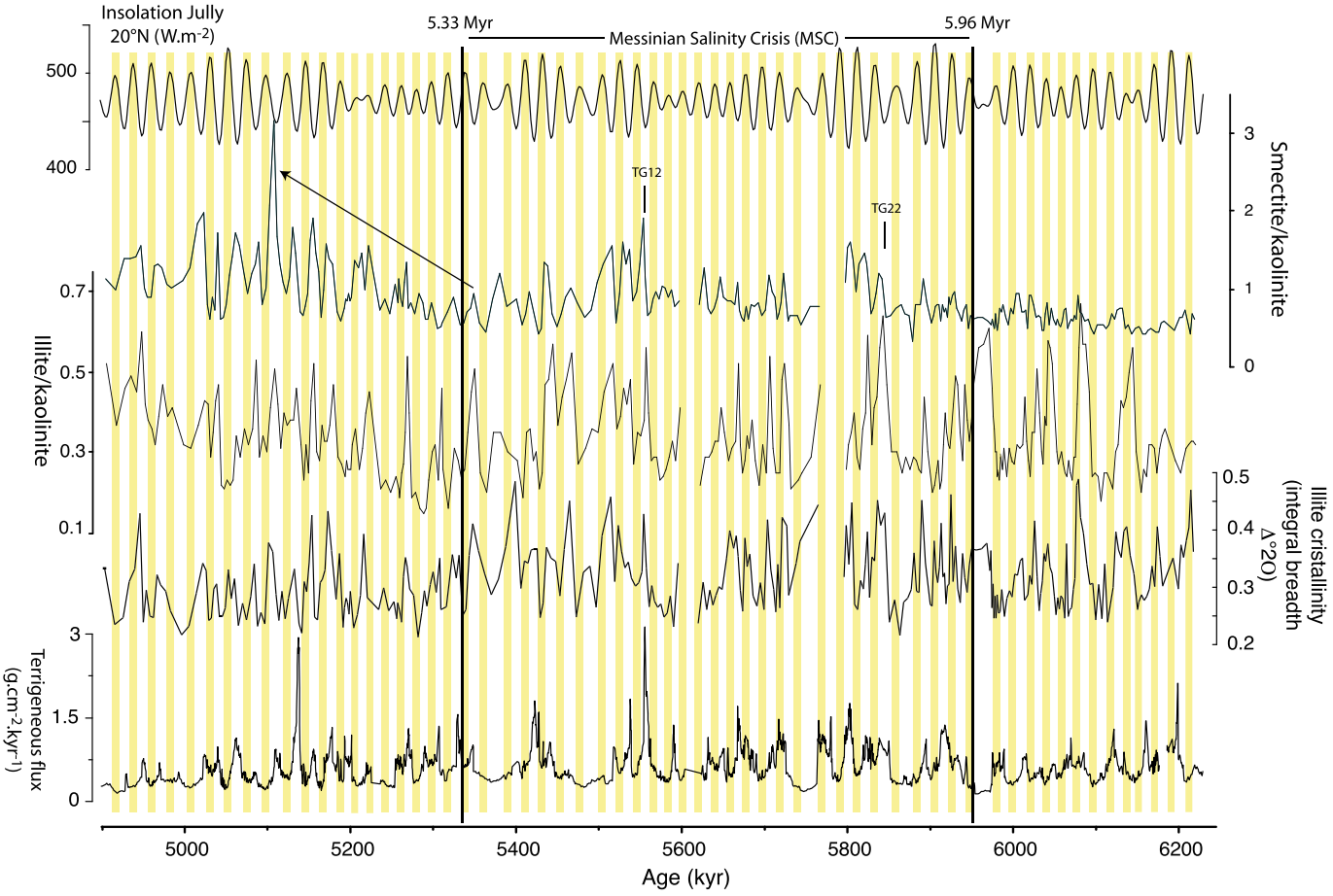

Fig. 4. Variations in smectite/kaolinite and illite/kaolinite ratios, Illite cristallinity and terrigeneous fluxes ($g.cm^{-2}.ka^{-1}$) versus age (kyr) for ODP Site 659. Insolation curve ($W.m^{-2}$) calculated for July at latitude of 20°N using the Analyseries software (Paillard et al., 1996) is also reported for comparison. Shaded bands denote intervals of maximum insolation.

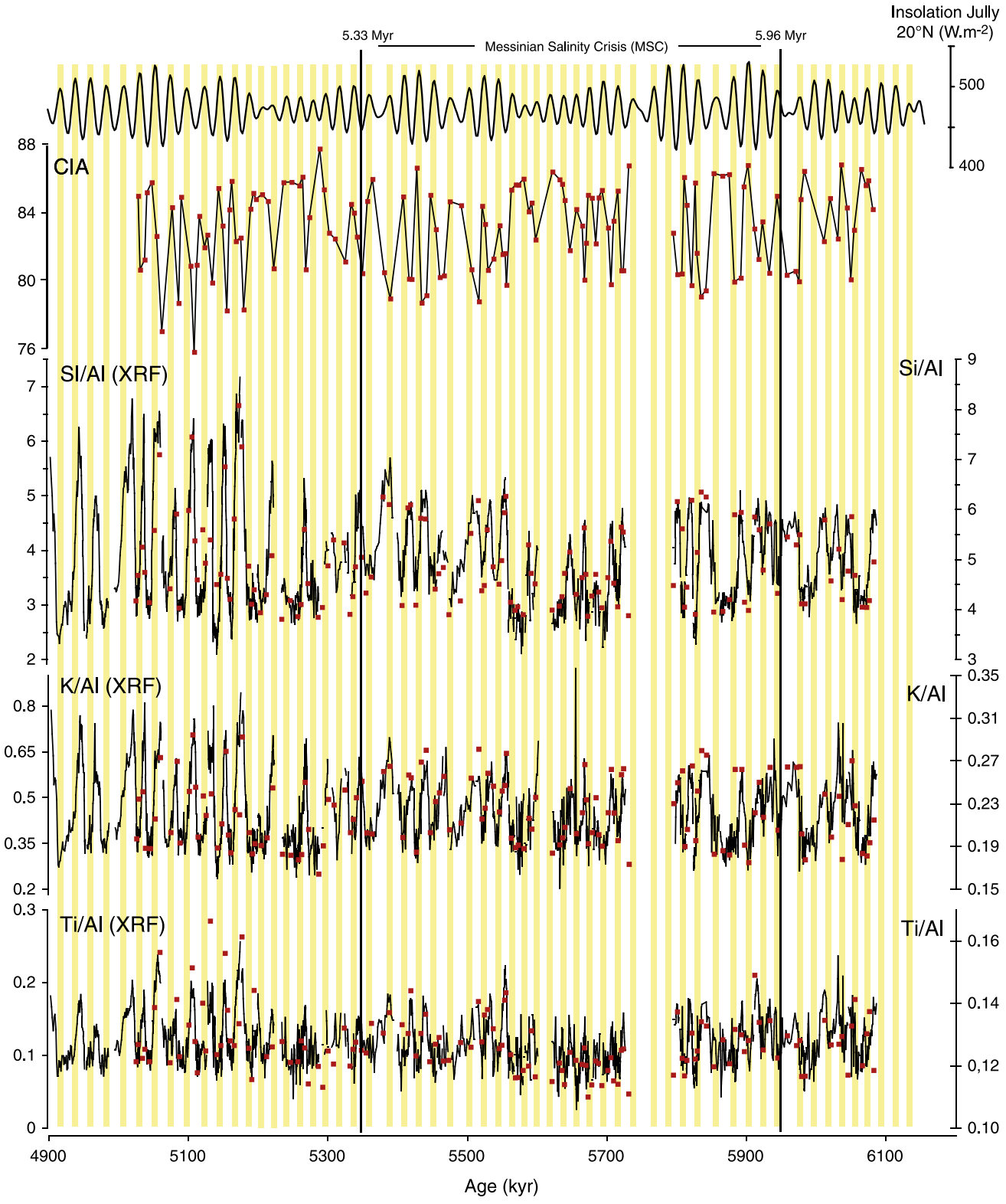

Fig. 5. Variations in Chemical index of alteration (CIA = $Al_2O_3/(Al_2O_3 + Na_2O + K_2O + CaO_{inorganic}) \times 100$), Si/Al, K/Al, Fe/Al and Ti/Al versus age (kyr) for ODP Site 659. The solid line corresponds to analysis obtained by XRF core-scanner. The red square corresponds to analysis carried out on discrete samples by ICP-OES. Insolation curve ($W.m^{-2}$) calculated for July at latitude of 20°N using the Analyseries software (Paillard et al., 1996) is also reported for comparison. Shaded bands denote intervals of maximum insolation.

affected by changes in physical properties for the studied interval depth of the ODP Site 659.

Variations in Si/Al, K/Al and Ti/Al at ODP Site 659, exhibit similar patterns, and closely match changes in clay mineralogy and the boreal summer solar radiation (Fig. 5). Each insolation curve minimum (maximum) is associated with an increase (a decrease) of these geochemical ratios. In general, a significant increase in the amplitude of the variations of the geochemical ratios is observed after 5.3 Myr in agreement with the long term-changes observed in the illite/kaolinite and smectite/kaolinite ratio records.

The Chemical Index of Alteration (CIA = molar ratio of [Al_2O_3/(Al_2O_3 + Na_2O + K_2O + CaOinorganic) × 100]) (Nesbitt and Young, 1982) was calculated on the basis of the major element compositions (Fig. 5). For primary minerals (non altered minerals), all feldspars have a CIA value of 50 and the mafic minerals – biotite, hornblende, and pyroxenes – have CIA values between of 50–55, 10–30, and 0–10, respectively. The weathering of Feldspar and mica to smectite and kaolinite results in a net loss of K and Na in weathering profiles, whereas Al is resistant and is enriched in weathering products (Nesbitt and Young, 1982). This induces an increase in CIA values of about 100 for kaolinite and 70–85 for smectite. The CIA value is thought to quantify the state of chemical weathering of the sediments by referencing the loss of labile elements such as Na, Ca, and K (Colin et al., 1999). For the ODP Site 659, the CIA values range from 75.8 to 87.7 and vary significantly with the solar radiation calculated at 20°N for July. Each of the insolation curve maxima (minima) corresponds to an increase (a decrease) of CIA indicating a significant increase of the state of chemical weathering of the ODP Site 659 sediments (Fig. 5).

4.4. Sr and Nd isotopes

$^{87}Sr/^{86}Sr$ ratios, εNd values and concentrations of Sr and Nd, measured on the ODP Site 659 carbonate-free fraction are listed in Table 1. Samples for Sr and Nd isotope analyses were selected in order to be representative of maxima and minima of the mineralogical, geochemical ratios and terrigenous flux records. εNd values present a narrow range from −14.5 to −13.6 and $^{87}Sr/^{86}Sr$ ranges from 0.7173 to 0.7186 implying a sediment that is derived from common crustal sources (Table 1). εNd and, more particularly, $^{87}Sr/^{86}Sr$ ratio values do not display any significant variations with respect to the changes in mineralogical and geochemical ratios previously described (Table 1).

5. Discussion

5.1. Sedimentary sources to the Cape Verde plateau

Located on top of the Cape Verde Plateau, 550 km offshore, the ODP Site 659 is distant from the main gravitary currents as well as from the possible reworked shelf sediments that might be transported during sea level lowering (Tiedemann et al., 1989; Wynn et al., 2000). In this particular sedimentary setting, previous studies performed on the Cape Verde Plateau have reported a dominant eolian component from the Sahara and Sahel zone (Tiedemann et al., 1994). In the present-day climatic context, the Sahara and Sahel areas constitute the most prominent source of dust in the world. Although dust particles are mainly produced in the Bodélé depression in Chad, the dust supplying the NEATO mainly originates from hot spots localised in the western Sahara, Mauritania, Mali, Niger and southern Algeria (Fig. 1; Goudie and Middleton, 2001; Skonieczny et al., 2013). The dust is mainly transported westward, both at high altitudes (5–6 km) during boreal summer by the Saharan Air Layer across the North Atlantic (Prospero and Nees, 1986), and at lower altitudes (1.5–3 km) during boreal winter-spring (Chiapello et al., 1995) by the northeast trade winds along the northwest African margin (also called Harmattan on the continent) (Fig. 1).

The range of terrigenous fluxes calculated for the studied time interval of Site 659 (between 0.14 to 2.13 $g.cm^{-2}.ka^{-1}$) are within the same order of magnitude as present-day eolian fluxes observed around the Cape Verde islands (1–2 $g.cm^{-2}.ka^{-1}$, Ratmeyer et al., 1999; Bory and Newton, 2000; Bory et al., 2003) suggesting a major contribution of eolian material to Site 659. Amplitudes of variations are also similar to those already observed by Tiedemann et al. (1994) prior to 5 Myr on Site 659. They have been attributed to past changes in the eolian dust input to the NEATO in relation to strong arid climate cycles in the South Sahara and Sahel Zone (Tiedemann et al., 1994). Considering that the average terrigenous flux between 6.2 to 4.9 Myr is two times lower than those of the late Quaternary, we can hypothesis that North Africa during the late Miocene to early Pliocene was characterised by relatively more humid conditions inducing less dust input to the NEATO. Here, the cyclic fluctuations of the terrigenous fluxes observed between 6.2 and 4.9 Myr are associated with mineralogical and geochemical variations allowing us to constrain the potential source areas of the terrigenous material, as well as the mode and strength of the transport processes involved.

The clay mineral assemblage of Site 659 (smectite ~35%, kaolinite ~41%, illite ~13%) also provides evidence that the main dust source is located in the southern Sahara–Sahel region rather than the northern Sahara, because illite is mainly derived from the northern sector while smectite and kaolinite are mostly from the south. To better understand the cause of cyclic fluctuations in palygorskite proportions as well as in smectite/kaolinite and illite/kaolinite ratios, it is necessary to document the origins and source areas of the minerals present in the dust and soils of North Africa. Distributions of kaolinite, illite and smectite in northwestern Africa exhibit a latitudinal distribution and are highly dependent on the efficiency of weathering processes in soils (Paquet et al., 1984). Illite dominates the clay assemblage of the northern sector of North Africa, and its relative abundance decreases gradually southward: illite constitutes ~ 60% of the clay mineral assemblage in northern Algeria, 50% in the central Sahara and less than 30% in the Sahelian zone (Paquet et al., 1984). In contrast, the kaolinite proportion exhibits low values in dusts deriving from northern Algeria and the westernmost part of North Africa, intermediate values in the central and southern Sahara, and high values in Sahelian regions (Pastouret et al., 1978; Paquet et al., 1984; Caquineau et al., 1998). Consequently, the illite/kaolinite ratio decreases markedly from north to south throughout the Saharan/Sahelian latitudinal band (Caquineau et al., 1998, 2002; Stuut et al., 2005). As the illite/kaolinite ratio is not affected by the various fractionation processes that occur during emission and long-range dust transport, it has been proposed that illite/kaolinite ratios are an efficient proxy for determining the latitudinal position of the dust sources (Caquineau et al., 1998). Palygorskite, a fibrous clay mineral characteristic of the sub-arid belt of the northern hemisphere (Chamley, 1989), can be distributed via eolian transport over long-range distances (Coudé-Gaussen et al., 1982; Molinaroli, 1996). It is mainly present in the northern part of West Africa, and is particularly abundant in the Anti-Atlas region of Morocco and in Tunisian loess (Grousset et al., 1992; Avila et al., 1997). Consequently, changes observed in the overall illite/kaolinite ratio and palygorskite content (Fig. 4), can be used as proxies for sedimentary provenance, indicating a latitudinal shift from a southern, Sahelian provenance areas during periods of low insolation to more northern, Saharan sources during periods of high summer isolation.

Smectite can also be used to track the origin of the sediment input to the NEATO (Stuut et al., 2005). Smectite, is indicative of wet tropical soils (e.g. Chamley, 1989), and is most abundant in a narrow band within the southern Sahara and Sahelian region (~20°N) where it can reach 70% of the clay assemblage. The smectite content in the fine fraction of northern African dust samples exhibits a high variability with ranges from 0 to 80%. Dust samples with high amounts of smectite mainly originate from southern Algeria, northern Mali and northern Niger (Paquet et al., 1984; Skonieczny et al., 2011, 2013). Finally, close to volcanic areas, smectite from deep-sea sediments could also derive from weathering of volcanic rocks (e.g. Chamley, 1989). Given the proximity of the Canary Islands to the study site, smectite could derive from the weathering of basalt outcrops on these islands and was then transported to the ODP Site 659 by the Canary current (Fig. 1).

The Nd isotopic composition and, to a lesser extent, the $^{87}Sr/^{86}Sr$ ratio can be used as reliable tracers for identifying the source of sediments deposited in the NEATO (Grousset et al., 1998; Colin et al., 2006; Cole et al., 2009; Meyer et al., 2011). It has been shown recently that $^{87}Sr/^{86}Sr$ of offshore sediments in north-western Africa are affected by grain size with more radiogenic values in the fine fraction (Dasch, 1969). In contrast, ε_{Nd} values are largely unaffected by grain size

Table 1
Sr and Nd concentrations, Sr and Nd isotopic composition measured on the carbonate-free fraction of ODP Site 659 sediments. Nd results have been expressed as $\varepsilon Nd(0) = [(^{143}Nd/^{144}Nd_{meas})/0.512638) - 1] \times 1000$, using the present-day CHUR value of *Jacobsen and Wasserburg* [1980]. Proportions of smectite (Sm), palygorskite (Pal), illite (Ill), kaolinite (Ka) and chlorite (Ch) as well as CIA are reported for comparison.

Leg	Site	Hole	Core	Sect.	Top (cm)	Bot (cm)	Depth (mbsf)	Depth (med)	Ages (kyr)	Sr (ppm)	±	Nd (ppm)	±	$^{87}Sr/^{86}Sr$	±2σ	$^{143}Nd/^{144}Nd$	±2σ	εNd	Sm (%)	Pa (%)	Ill (%)	Ka (%)	Ch (%)	CIA (%)
108	659	B	16H	3	92	94	139.52	143.11	5107.7	124.6	0.0	24.9	0.3	0.718164	0.000032	0.511894	0.000006	−14.5	62	2	10	19	7	75.8
108	659	B	16H	3	132	134	139.92	143.51	5122.9	114.2	0.0	24.7	0.5	0.717936	0.000032	0.511906	0.000006	−14.3	37	5	13	36	9	82.0
108	659	B	16H	4	12	14	140.22	143.81	5133.9	292.2	0.0	36.0	1.1	0.717536	0.000032	0.511907	0.000006	−14.3	45	5	13	29	9	79.9
108	659	B	16H	4	42	44	140.52	144.11	5142.9	103.9	0.7	24.6	0.5	0.717715	0.000032	0.511894	0.000005	−14.5	33	4	10	44	9	85.4
108	659	B	16H	4	82	84	140.92	144.51	5154.9	136.8	0.1	26.2	0.2	0.717880	0.000032	0.511939	0.000008	−13.6	51	3	13	25	7	78.3
108	659	B	16H	4	101.5	103.5	141.115	144.705	5161.9	109.8	0.3	24.4	0.0	0.717308	0.000032	0.511924	0.000006	−13.9	45	3	9	34	10	85.9
108	659	B	18H	4	110	112	160.2	164.82	6045.6	116.4	0.5	20.6	1.2	0.718411	0.000032	0.511926	0.000006	−13.9	25	6	22	39	8	84.3
108	659	B	18H	5	5	7	160.65	165.27	6066.1	139.9	0.3	23.7	1.5	0.718568	0.000032	0.511917	0.000006	−14.1	36	1	10	43	10	86.6
108	659	B	18H	5	45	47	161.05	165.67	6082.8	121.2	2.4	21.3	1.5	0.717308	0.000032	0.511941	0.000007	−13.6	27	5	23	34	12	84.2
108	659	B	18H	5	90	92	161.5	166.12	6107.3	97.5	1.3	24.4	0.8	0.718683	0.000032	0.511909	0.000006	−14.2	27	1	11	46	15	86.7

(e.g., Meyer et al., 2011) and chemical weathering processes (Colin et al., 1999, 2006). As Sr and Nd isotope analyses have been carried out on the bulk terrigenous fraction, they could reflect changes in particle size and mixing proportions of sediment subpopulations deriving from different sedimentary sources. Nevertheless, the presence of any small contribution of volcanic material in sediment from the ODP Site 659 could be marked by an unradiogenic Sr isotopic composition independently of any grain-size effect (e.g. Grousset et al., 1998; Boulay et al., 2005). The $^{87}Sr/^{86}Sr$ and ε_{Nd} values reveal narrow ranges (εNd between −14.5 and −13.6; $^{87}Sr/^{86}Sr$ between 0.7173 and 0.7186; Table 1) similar to Sr and Nd isotopic compositions obtained in several previous studies of surface sediments located off Mauritania and Senegal ($^{87}Sr/^{86}Sr$ between 0.715 and 0.723; εNd between −12.2 and −15.1) (Grousset et al., 1998; Meyer et al., 2011; Scheuvens et al., 2013). In addition, high smectite contents in sediments from Site 659 are not associated with a significant decrease in the $^{87}Sr/^{86}Sr$ ratio and/or an increase of the εNd values. This implies that the smectite cannot derive from the weathering of young volcanic rocks on the Canary Islands. In addition, the inferred clay mineralogical record reveals that most of the higher smectite contents are associated with an increase in the proportion of illite and palygorskite as well as an increase in the terrigenous fluxes (assumed to be of eolian origin) suggesting similar sedimentary sources. This is in agreement with previous studies that have shown that volcanic material in surface sediments of the NEATO is mainly deposited around the Canary Islands (Grousset et al., 1998; Govin et al., 2012; Scheuvens et al., 2013). Consequently, taking into consideration that the studied area is not affected by the input of mafic rock material, an increase in the smectite/kaolinite ratio is likely to reflect a modification of the sediment provenance within North Africa. An increase in the smectite/kaolinite ratio would therefore imply inputs of sediments deriving from northern latitudes, whereas a decrease in the smectite/kaolinite ratios would indicate sediments deriving mostly from the Sahelian region where laterite soils are dominated by kaolinite (e.g. Chamley, 1989).

Sr and Nd isotopic composition analyses have been conducted on dusts and soil samples from possible source sediments enabling us to identify the main source regions in northern Africa (e.g. Grousset and Biscaye, 2005; Skonieczny et al., 2011; Scheuvens et al., 2013; Skonieczny et al., 2013). Taking into account that our samples are not sieved, we cannot make direct comparisons with $^{87}Sr/^{86}Sr$ ratios available in the literature for this area (generally fraction <30–40 μm). However, εNd obtained in the ODP Site 659 are within the range of eolian particles collected during major dust events at the Mbour station (about 80 km south of Dakar, Fig. 1; Skonieczny et al., 2011, 2013) and off Mauritania and Senegal (Meyer et al., 2011). These sites display εNd values between −13 and −15. This indicates that sediments from the ODP Site 659, for the studied time period, probably derive from a mixture of sources including areas of northwest Africa (low topographic) that cover parts of the western Sahara, Mauritania, Mali, Niger and southern Algeria (Goudie and Middleton, 2001; Skonieczny et al., 2013). These areas correspond to the Potential Source Area (PSA) 2 and 3 as defined in present-day nomenclature for the North African sources (Formenti et al., 2011; Scheuvens et al., 2013).

In addition, Si/Al and K/Al ratios in the Cape Verde plateau sediments are strongly correlated ($R^2 = 0.86$). Si/Al and Ti/Al ratio are also well correlated ($R^2 = 0.82$). These findings suggest that Si, Ti and K could derive from the same sources of sediment. Given that wind-blown dusts from the Sahara collected off the Cap Verde are mostly composed of quartz, micas, feldspar and clay minerals (Wilke et al., 1984), ratios of Si/Al and K/Al have been used to establish past changes in Saharan dusts. Such an approach has been already used in the context of Mediterranean Sea sediments (e.g. Wehausen and Brumsack, 1999; Calvert and Fontugne, 2001; Zhao et al., 2012) and can thus be adopted to investigate intensities of dust activities.

The K/Al ratio in dust and source sediments results primarily from leaching and depletion of K during the weathering of soils. In general,

highly weathered soils, characterised by depleted labile elements such as Na, Ca, Si and K and by high CIA values, are located in tropical African regions where annual rainfall is high. In contrast, moderately weathered soils are present in the northern Sahara, characterised by arid and hyperarid conditions. Chiapello et al. (1997) have shown that Si/Al and K/Al ratios in dust decrease gradually from the North Sahara, through the South Sahara to the Sahel. In addition, lower Si/Al and K/Al ratios than those associated with Saharan dust have been observed in suspended material from the Senegal and the Niger Rivers where the catchments are composed of intensively weathered, kaolinite-rich soils (high Al content) (Martin and Meybeck, 1979; Gaillardet et al., 1999). Consequently, Si/Al and K/Al can be used to track eolian input to the NEATO and are related to the latitudinal position of the sedimentary source.

In addition, Ti is enriched in several heavy minerals present in the Sahara dust (e.g. ilmenite, anatase, rutile, and titanomagnetite). Despite an increase in Ti content in aerosol samples from the Bodélé depression (Bristow et al., 2010), the distribution of Ti content does not exhibit any regional trend and cannot be used as a source marker to discriminate between different eolian sedimentary source areas in northern Africa (Scheuvens et al., 2013). However, Ti/Al has been already used to track eolian input to the ocean (e.g. Wehausen and Brumsack, 1999) and the distribution of Ti/Al in NEATO sediments displays high values in areas of high dust deposition deriving from the Sahara and low values in regions dominated by the input of suspended material from the Senegal and Niger rivers (Govin et al., 2012).

In summary, since ODP site 659 is not affected by the input of mafic material from the volcanic islands, an increase in Si/Al, K/Al and Ti/Al ratios, associated with a decrease in CIA values and an increase in terrigenous fluxes, imply a higher proportion of eolian dust deriving from the arid desert of North Africa (Figs. 5 and 7).

5.2. ITCZ-modulated variations of the clay mineralogy and African monsoon activity

A spectral analysis has been performed using Analyserie software (Paillard et al., 1996) on mineralogical and geochemical ratio records from the ODP Site 659. The power density spectrum reported in Fig. 6 shows significant periodicities at 19, 23, 41 and 61 kyr for the illite/kaolinite ratio and at 19, 23, 41 and 51 kyr for the smectite/kaolinite ratio. The K/Al, Ti/Al and Si/Al ratios display periodicities at 19, 23, 54, 41 kyr and, to a lesser extent, at 100 kyr. Periodicity at 23 and 19 kyr is attributed to the precessional changes of the Earth's orbit, and periodicities close to 41 kyr are related to long-term changes in the ice-volume at the studied time interval. The periodicity in the eccentricity change at ca. 100 kyr is not well marked in the time interval studied at Site 659. A dominance of the periodicities corresponding to orbital precession (23 and 19 kyr) have already been observed in several detrital records from the NEATO for the time interval between 4.5 and 2.8 Myr (Tiedemann et al., 1994; deMenocal, 1995a,b, 2004). Changes in these mineralogical and geochemical ratios show congruent precession-related (23 kyr) oscillations correlating the mineralogical characteristics with the solar radiation calculated at 10°N for July (Figs. 5 and 7). The smectite/kaolinite record is also well correlated to the summer insolation curve particularly after 5.3 Myr when the amplitude of the smectite/kaolinite variations increases strongly. These results suggest that mineralogical and geochemical ratio variations are strongly related to changes in the African monsoon.

Previous studies have suggested that the dust production rate in arid regions is closely related to annual precipitation (Pye, 1989; Rea, 1994). Precipitation changes in North Africa are, however, generally modulated by the position of the ITCZ (Camberlin et al., 2001). The seasonal migration of the ITCZ is a direct response to changes in the location of maximum solar heating. As a result, there exists a northern-hemisphere belt and southern-hemisphere belt of monsoonal climates with summer rains and winter drought, bracketing a humid equatorial zone characterised by a double rainfall maximum annually (Gasse, 2000). As long-term changes of the ITCZ location are modulated by the Earth's astronomical precession (Laskar et al., 2004), there may also exist an equatorial zone characterised by double rainfall maximum in each precessional cycle. Therefore, aridity in North Africa, and thus dust production in the Sahara, is predominantly controlled by changes in the location of the ITCZ. As variations in the clay assemblage in north-western African dust sources are highly latitudinal, migration of the ITCZ can have a strong impact on the clay mineralogy of dusts derived from the Sahara. This has been illustrated recently by observations made at the Mbour station where seasonal variations in the illite/kaolinite ratio of dust have been associated with a seasonal migration of the ITCZ (Skonieczny et al., 2013).

During intervals of low summer insolation, the increase in terrigenous fluxes, combined with higher values of illite/kaolinite, Si/Al and K/Al ratios and low CIA values, suggest a southern position for the ITCZ, an aridification of the Saharan region, an increase in dust emission from the Sahara and Sahel region and an intensification of eolian dust input from the Sahara to Site 659 (Fig. 7). This time interval is also systematically associated with an increase in the illite crystallinity index which also suggests dust emission from a region characterised by moderate hydrolysis conditions. Such conditions permit the formation of open illite (e.g. Chamley, 1989). These findings also suggest a different source of illite derived from wind erosion of low latitude soils.

During wet periods of summer monsoon (time intervals of high summer insolation), the terrigenous fluxes decrease drastically implying a reduction in eolian dust (Tiedemann et al., 1994). This time interval is also associated with low smectite/kaolinite and illite/kaolinite ratios as well as low Si/Al, K/Al and Ti/Al ratios and high CIA values implying a higher relative proportion of sediments derived from the Sahel and sub-tropical regions and a decrease in detrital material derived from the northern part of the Sahara (Fig. 7). During such periods, the northward shift of the ITCZ accounts for a drastic reduction in eolian input (illite and palygorskite) from the southern Sahara which is covered by vegetation ("green Sahara") as has been demonstrated for a different time intervals during the Quaternary (e.g. Gasse, 2000). The northward shift of the ITCZ would induce a northward displacement of the eolian sources mainly to the North Sahara favouring a decrease in the eolian dust supplying the Cape Verde plateau. The decrease in the illite crystallinity index observed in Site 659 during times of high summer insolation could reflect a minor contribution of illite from a region characterised by very low hydrolysis conditions such as those observed at the present time in the northern Sahara. As kaolinite content from Site 659 increases when the ITCZ reaches its highest latitudinal position, we suggest that kaolinite was primarily transported to the studied site by fluvial supply via African rivers. In fact, it has been shown that during wet periods such as African Humid Periods, the watershed of the Senegal River was greatly extended and potential paleorivers, such as the Tamanrasset river, whose mouth was located on the Mauritanian coast and directly connected with the NEATO, were probably re-activated thus transferring large amounts of terrigenous particles to the ocean (e.g., Vörösmarty et al., 2000). Further Sr and Nd isotopic analyses will be necessary on selected grain size fractions, including clay, to throw light on such drastic modification of the sedimentary sources.

5.3. Relations between climate changes and the Messinian Salinity Crisis

The Messinian Salinity Crisis (MSC) is characterised by the deposition of a large volume of evaporites (1500 m) in the Mediterranean Basin (Hsü et al., 1973) during a short time-interval (5.96–5.33 Myr: Gautier et al., 1994; Krijgsman et al., 1999a) and implies major paleogeographical changes in the Mediterranean basin. Since the discovery of this event (Hsü et al., 1973), two groups of conceptual scenarios have been proposed to explain the deposition of these evaporites (Butler et al., 1995; Clauzon et al., 1996; Krijgsman et al., 1999a,b;

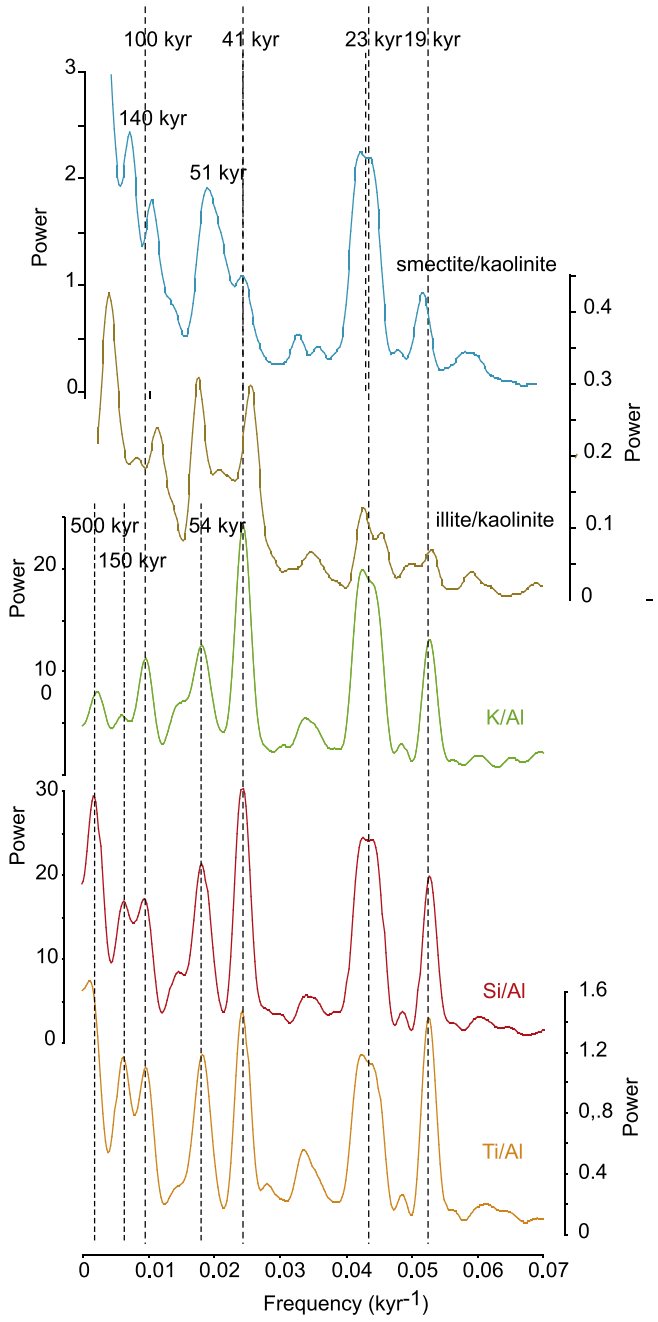

Fig. 6. Periodograms of smectite/kaolinite, illite/kaolinite, K/Al, Fe/Al, Si/Al and Ti/Al from ODP Site 659. The mean temporal resolution of the mineralogical and geochemical ratios performed by spectral analyses are 4 and 0.52 kyr, respectively.

Rouchy and Caruso, 2006). The first group of scenarios favours a synchronous deposition (at 5.96 My) of the first evaporites throughout the Mediterranean basin before the massive fall in sea level (Krijgsman et al., 1999a,b; Rouchy and Caruso, 2006; De lange and Krijgsman, 2010) while the second group favours a diachronous deposition of the evaporites through two phases of desiccation (Butler et al., 1995; Clauzon et al., 1996; Riding et al., 1998; Butler et al., 1999). All of these scenarios envisage the almost complete isolation of the Mediterranean Sea due tectonic activity which leads to the closure of the gateways between the Atlantic and the Mediterranean (Krijgsman, 2002; Duggen et al., 2003). This event is associated with major paleogeographical changes that begin with a huge sea-level fall of the Mediterranean Sea (at least 1500 m; Clauzon, 1982), probably in several steps, after 5.6 Myr (Lofi et al., 2005; Maillard et al., 2006; Gargani and Rigollet, 2007) and ends with the catastrophic marine re-flooding at 5.33 Myr. Several studies based on numerical models, or on the organisation of the Messinian deposits, have shown a fast re-flooding of the Mediterranean Sea at least during its terminal phase at the end of the Salinity Crisis (5.33 Ma) (e.g. Blanc, 2002; Lofi et al., 2005; Loget et al., 2005; Garcia-Castellanos et al., 2009).

Despite recent progress regarding the chronology of the MSC, correlations between major events of the crisis and climatic records still remain poorly documented. It was proposed that the MSC was not associated with major climatic modification (Warny et al., 2003; Bertini, 2006) even though more humid climatic conditions have been locally observed in the Mediterranean Sea (Griffin, 2002; Willett et al., 2006; Gladstone et al., 2007). More recently, a compilation of pollen records collected around the Mediterranean basin indicates that the MSC event does not seem to be at the origin of climate modifications in the Mediterranean region, particularly in the south-western area, where the climate was dry and warm before, during and after the event (Fauquette et al., 2006). At present, climatic variations during the MSC over North Africa are not well established in spite of its potential impact on freshwater input to the Mediterranean Sea by North African rivers. Indeed, this fresh water discharge could explain deep valley incisions and large delta deposits (Lofi et al., 2005; Bache et al., 2010) and part of the evaporite accumulation in the deep basin (Gargani et al., 2008; Topper and Meijer, 2013).

The well-established chronology for ODP Site 659 allows us, for the first time, to make a comparison between the major events of the MSC and the evolution of North African monsoon intensity. For the ODP Site 659, long-term changes in smectite/kaolinite, Si/Al, K/Al and Ti/Al ratios and, to a lesser extent, illite/kaolinite ratios indicate a significant modification around 5.3 Myr, coeval with the end of the MSC. After 5.3 Myr, the smectite/kaolinite ratios increase significantly and present higher amplitudes of variations well correlated to the summer insolation curve (Figs. 5 and 7). This increase in the smectite/kaolinite ratio is also associated with an increase in the amplitude of variations of Ti/Al, K/Al and Si/Al ratios. These variations suggest a modification of the sedimentary sources for the dust. At the present time, the smectite content in the clay fraction of northern African dust samples shows a wide range of values. Smectite is most abundant in a narrow band in the southern Sahara and Sahelian region (~20°N). In Tanezrouft (a region between Hoggar and Adrar des Iforhas) and Cape Blanc (between Mauritania and Western Sahara), the proportion of the smectite can reach 70%. Apart from some areas in southern Libya, dust sources in the central and northern Sahara are depleted in smectite (Avila et al., 1997). Consequently, we suggest that eolian sources containing a high proportion of smectite (~20°N, Fig. 1) become more active after 5.3 Myr and during the intervals with a boreal summer insolation minimum.

Such results imply a long-term southward migration of the ITCZ after 5.3 Myr. Before 5.3 Myr, we suggest that the ITCZ seasonal migration is north of 20°N. Such a northward migration of the ITCZ does not permit strong inputs to site 659 of dust derived from the present-day narrow, smectite-rich band (~20°N). After 5.3 Myr, the ITCZ migrates southward inducing a decrease in the vegetation cover of the southern Sahara and Sahelian region. It also results in arid conditions in the region characterised by smectite-rich soils (mainly the Bodélé depression in northern Chad) and in an area covering eastern Mauritania, western Mali and southern Algeria which, in turn, induces the emission and transport of particularly smectite-rich dust to Site 659. The high relative content of illite and palygorskite during this time interval suggests that the Sahara source was still active. In contrast, the decrease in kaolinite content after 5.3 Myr suggests a reduction in monsoon rainfall and an associated decrease in runoff of kaolinite from tropical soil and in its transport by rivers to the study site.

The northward position of the ITCZ observed in the clay record of the ODP Site 659 before 5.3 Myr is in agreement with recent observations on the genesis of numerous incised valleys in the Abu Madi Valley

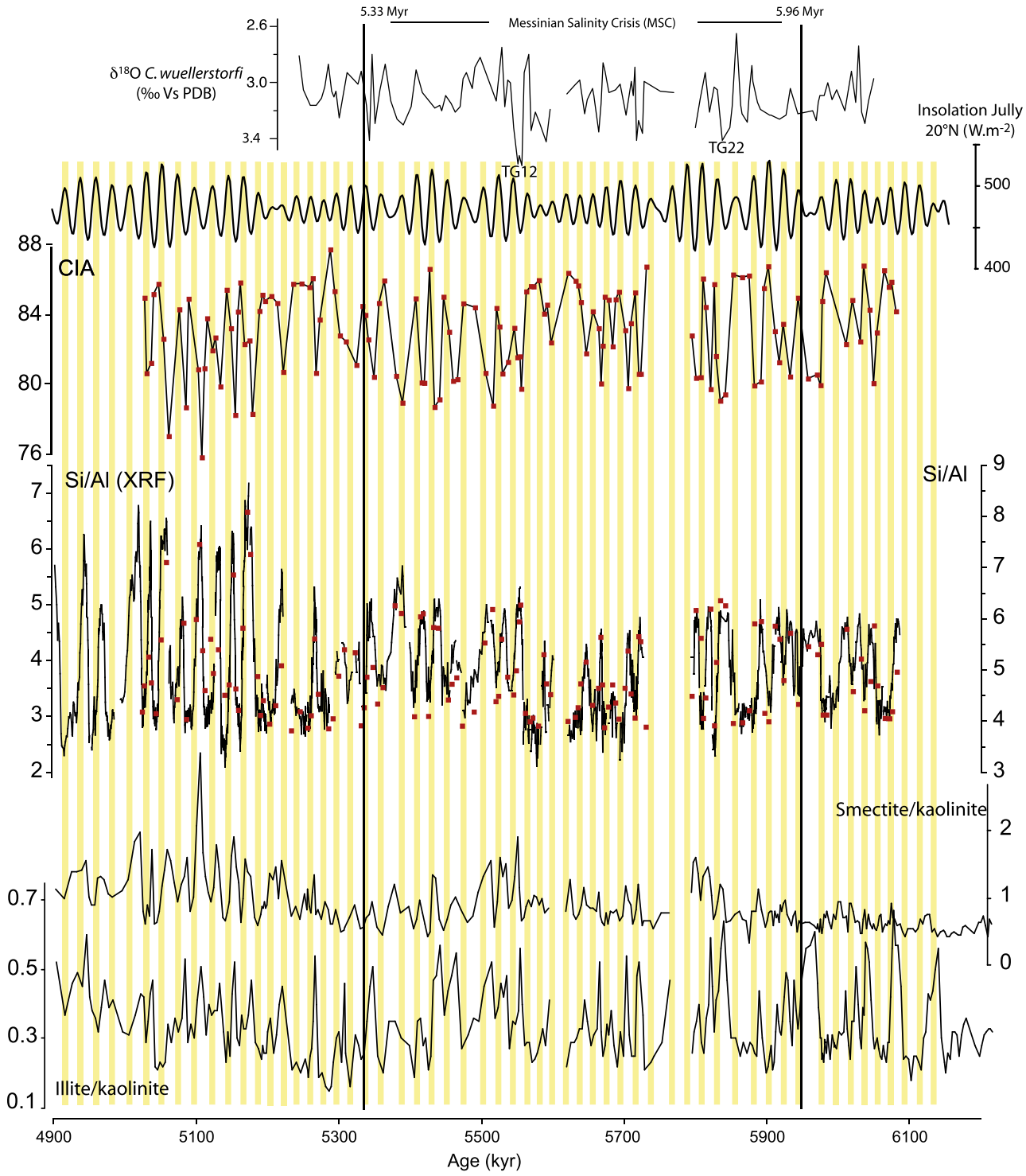

Fig. 7. Variations in Chemical index of alteration (CIA = $Al_2O_3/(Al_2O_3 + Na_2O + K_2O + CaOinorganic) \times 100$), Si/Al, smectite/kaolinite ratio and illite/kaolinite ratio versus age (kyr) for ODP Site 659. Insolation curve ($W.m^{-2}$) calculated for July at latitude of 20°N using the Analyseries software (Paillard et al., 1996) is also reported for comparison. Shaded bands denote intervals of maximum insolation.

during the MSC suggesting heavy rainfall in the northern part of North Africa (Gargani et al., 2010). In addition, the dust flux record of the Arabian Sea ODP Sites 721/722 indicates a significant decrease in dust input to the Arabian Sea between 5.9 and 5.3 Myr suggesting humid conditions in north-eastern Africa and Arabia during the MSC (Griffin, 1999, 2002; Paillou et al., 2009).

Gladstone et al. (2007) have performed several sensitivity experiments using an Atmospheric General Circulation Model (AGCM). The model conditions were forced by using Late Miocene global paleogeography, a higher CO_2 concentration and a different SST distribution for the late Miocene. Results indicate a strong northward shift in the ITCZ caused by a reduced latitudinal gradient in global sea surface temperatures. This provides a large positive net precipitation–evaporation balance over North Africa which is very pronounced to a latitude of 25°N, in agreement with results obtained on the ODP Site 659 before and during the MSC. Furthermore, the global climate at the end of the MSC is not

associated with high latitude cooling. Vidal et al. (2002) indicate that the second phase of evaporite deposition must have occurred during a period of global warming and that the end of the MSC was not associated with a glacial cooling. $\delta^{18}O$ records obtained from benthic foraminifera from the ODP Site 659 confirm this scenario at the end of the MSC. Two main $\delta^{18}O$ excursions, marked by the highest values, correspond to the major glacial stages TG22 and TG12 dated respectively at 5.84 and 5.55 Myr in agreement with the results of the previous studies (Shackleton et al., 1995; Shackleton and Crowhurst, 1997; Hodell et al., 2001). These cold events are associated with an increase in the smectite/kaolinite ratios in the ODP Site 659 and are indicative of a significant southward migration of the ITCZ during the MSC. In addition, the global warming period observed after 5.56 Myr is not associated to any modification of the mineralogical ratios on the ODP Site 659.

More recently, Murphy et al. (2009) and Schneck et al. (2010) have investigated climate sensitivity to the lowering of the Mediterranean surface and to the surface transition from sea to land. They found that there were significant climate changes over North Africa in response to these modifications. In winter, the lowering of the sea level of the Mediterranean Sea lead to a strengthening of wind velocity flowing southward along North West Africa (Murphy et al., 2009). Such a wind pattern could be responsible for the presence of eolian dust, characterised by illite and palygorskite, from North West Africa (Morocco, North-West Sahara). In contrast, summer is characterised by an intensification of rainfall over North Africa responsible for the net positive precipitation–rainfall balance anomaly over North East Africa. Such modification could be responsible for an increase in vegetation cover and for a reduction in smectite transported by wind from the southern Sahara and Sahelian region (~20°N) to the NEATO.

The northern position of the ITCZ before the re-flooding of the Mediterranean Sea may be responsible for increased Late Miocene river discharge from North Africa into the Mediterranean basin. This fresh water discharge must be taken into account when considering the freshwater budget during the MSC and may explain part of the evaporite accumulation in the deep basin (Gargani et al., 2008). We propose that the re-flooding of the Mediterranean Sea at the end of the MSC could be responsible for a reorganisation of the regional atmospheric circulation with a displacement of the low-pressure cells over North Africa, a southward shift of the ITCZ, and greater aridity in the Sahara region. Further climatic records covering North Africa during the MSC need to be investigated to better constrain the migration of the ITCZ and to determine the exact timing and amplitude of the ITCZ migration during this period.

6. Conclusion

An orbital time scale has been established for ODP Site 659 located on the Cap Verde plateau between 6.2 to 4.9 Myr. Terrigenous fluxes combined with clay mineralogy (smectite/kaolinite, illite/kaolinite), major elements (Si/Al, K/Al and Ti/Al) and Sr and Nd isotopic composition of the detrital sediment allow us to establish a strong relationship between detrital input to the Cap Verde plateau and the position of the seasonal migration of the ITCZ (African monsoon rainfall distribution over North Africa).

At a millennial time scale, periods of low summer insolation are characterised by greater aridity in the Saharan regions induced by a southern position of the ITCZ. This, in turn, is responsible for the input of dust characterised by high illite and smectite contents, low CIA and high Si/Al, K/Al and Ti/Al ratios. Periods of high summer insolation are associated with a northern shift of the ITCZ inducing a drastic reduction in the eolian input and an intensification of sediment derived mainly from the Senegal River and potential paleo-rivers, such as the Tamanrasset river, which are characterised by high chemical weathering states (high content of kaolinite, high CIA and low K/Al).

At longer time scales, smectite/kaolinite, Si/Al, K/Al and Ti/Al ratios and, to a lesser extent, illite/kaolinite ratios display significant modification suggestive of a change in sedimentary source around 5.3 Myr, coeval with the end of the MSC. After 5.3 Myr, the smectite/kaolinite ratios increase significantly and present higher amplitudes of variation also associated with an increase in the amplitudes of variation of Ti/Al K/Al and Si/Al ratios. As smectite is most abundant in soils and dusts deriving from the southern Sahara and Sahelian region (~20°N band of latitude), such mineralogical changes suggest a northward shift of the ITCZ before and during the MSC and a long-term southward migration of the ITCZ after the re-flooding of the Mediterranean Sea (~5.3 Myr). These results indicate, for the first time, that significant changes in the paleogeography of the Mediterranean Sea at the end of the MSC induced a re-organisation of the atmospheric circulation and drier conditions over North Africa. This is in agreement with recent modelling experiments that indicate the existence of humid climatic conditions over North Africa when the paleogeography of the Mediterranean Sea was modified with the replacement of the sea by land surface (Murphy et al., 2009; Schneck et al., 2010).

Acknowledgements

Remy Pichon and Olivier Dufaure are warmly thanked for their technical assistances in XRD analyses. The two anonymous reviewers are also thanked for constructive comments on the manuscript.

References

Avila, A., Queralt-Mitjans, I., Alarcón, M., 1997. Mineralogical composition of African dust delivered by red rains over northeastern Spain. J. Geophys. Res. 102, 21977–21996.
Bache, F., Olivet, J.-L., Gorini, C., Aslanian, D., Labails, C., Rabineau, M., 2010. Evolution of rifted continental margins: the case of the Gulf of Lions (Western Mediterranean Basin). Earth Planet. Sci. Lett. 292, 345–356.
Backman, J., Raffi, I., 1997. Calibration of Miocene nannofossil events to orbitally tuned cyclostratigraphies from Ceara rise. Proc. ODP Sci. Results 154, 83–99.
Bertini, A., 2006. The Northern Apennines palynological record as a contribute for the reconstruction of the Messinian palaeoenvironments. Sediment. Geol. 188–189, 235–258.
Blanc, P.L., 2002. The opening of the Plio-Quaternary Gibraltar Strait: assessing the size of a cataclysm. Geodin. Acta 15, 303-317.e.
Bory, A.J.-M., Newton, P.P., 2000. Transport of airborne lithogenic material down through the water column in two contrasting regions of the eastern subtropical North Atlantic Ocean. Global Biogeochemical Cycles, 14. http://dx.doi.org/10.1029/1999GB900098 (0886–6236).
Bory, A.J.-M., Biscaye, P.E., Grousset, P.E., 2003. Two distinct seasonal Asian source regions for mineral dust deposited in Greenland (NorthGRIP). Geophys. Res. Lett. 30, 1167.
Boulay, S., Colin, C., Trentesaux, A., Frank, N., Liu, Z., 2005. Sediment sources and East Asian monsoon intensity over the last 450 ky. Mineralogical and geochemical investigations on the South China Sea sediments. Palaeogeogr. Palaeoclimatol. Palaeoecol. 228, 260–277.
Bristow, C.S., Hudson-Edwards, K.A., Chappell, A., 2010. Fertilizing the Amazon and Equatorial Atlantic with West African dust. Geophys. Res. Lett. 37, L14807. http://dx.doi.org/10.1029/2010GL043486.
Butler, H., Lickorish, W.H., Grasso, M., Pedley, H.M., Ramberti, L., 1995. Tectonics and sequence stratigraphy in Messinian basins, Sicily: constraints on the initiation and termination of the Mediterranean salinity crisis. Geol. Soc. Am. Bull. 107, 425–439.
Butler, R.W.H., McClelland, E., Jones, R.E., 1999. Calibrating the duration and timing of the Messinian salinity crisis in the Mediterranean: linked tectonoclimatic signals in thrust-top basins of Sicily. J. Geol. Soc. Lond. 156, 827–835.
Calvert, S.E., Fontugne, M.R., 2001. On the late Pleistocene–Holocene sapropel record of climatic and oceanographic variability in the eastern Mediterranean. Paleoceanography 16, 78–94.
Calvert, S.E., Pedersen, T.F., 2007. Elemental proxies for palaeoclimatic and palaeoceanographic variability in marine sediments: interpretation and application. In: Hillaire-Marcel, C., De Vernal, A. (Eds.), Proxies in Late Cenozoic Paleoceanography. Elsevier, Amsterdam, pp. 567–644.
Camberlin, P., Janicot, S., Poccard, I., 2001. Seasonality and atmospheric dynamics of the teleconnection between African rainfall and tropical sea-surface temperature: Atlantic vs ENSO. Int. J. Climatol. 21, 973–1005.
Caquineau, S., Gaudichet, A., Gomes, L., Magonthier, M.-C., Chatenet, B., 1998. Saharan dust: clay ratio as a relevant tracer to assess the origin of soil-derived aerosols. Geophys. Res. Lett. 25, 983–986.
Caquineau, S., Gaudichet, A., Gomes, L., Legrand, M., 2002. Mineralogy of Saharan dust transported over northwestern tropical Atlantic ocean in relation to source regions. J. Geophys. Res. 107 (D15), 12.
Chamley, H., 1989. Clay Sedimentology. Springer Publishing, Berlin.
Chiapello, I., Bergametti, G., Gomes, L., Chatenet, B., Dulac, F., Pimenta, J., Suares, E.S., 1995. An additional low layer transport of Sahelian and Saharan dust over the north-eastern tropical Atlantic. Geophys. Res. Lett. 22 (23), 3191–3194. http://dx.doi.org/10.1029/95GL03313.

Chiapello, I., Bergametti, G., Chatenet, B., Bousquet, P., Dulac, F., Santos Soares, E., 1997. Origins of African dust transported over the northeastern tropical Atlantic. J. Geophys. Res. Atmos. 102 (D12), 13701–13709.
Clauzon, G., 1982. The Messinian Rhone canyon as a definite proof of the "dessicated deep-basin model". Bull. Soc. Geol. Fr. XXIV, 597–610.
Clauzon, G., Suc, J.P., Gautier, F., Berger, A., Loutre, M.F., 1996. Alternate interpretation of the Messinian salinity crisis: controversy resolved? Geology 24, 363–366.
Cole, J.M., Goldstein, S.L., deMenocal, P.B., Hemming, S.R., Grousset, F.E., 2009. Contrasting compositions of Saharan dust in the eastern Atlantic Ocean during the last deglaciation and African Humid Period. Earth Planet. Sci. Lett. 278, 257–266.
Colin, C., Turpin, L., Bertaux, J., Desprairies, A., Kissel, C., 1999. Erosional history of the Himalayan and Burman ranges during the last two glacial-interglacial cycles. Earth Planet. Sci. Lett. 171, 647–660.
Colin, C., Turpin, L., Blamart, D., Frank, N., Duchamp, S., 2006. Evolution of weathering patterns in the Himalayas and Indo-Burman ranges over the last 280 kyr: effects of sediment provenance on $^{87}Sr/^{86}Sr$ ratios tracers. Geochem. Geophys. Geosyst. 7, Q03007. http://dx.doi.org/10.1029/2005GC000962.
Colin, C., Siani, G., Segueni, F., Blamart, D., Giuta, S., Suc, J.P., Liu, Z., Frank, N., Briqueu, L., 2008. Reconstruction of Northern African monsoon at the Mio-Pliocene; relationships with the Messinian Salinity Crisis. CR Acad. Sci. Paris 340, 749–760. http://dx.doi.org/10.1016/j.crte.2008.07.005.
Coplen, T.B., Kendall, C., Hopple, J., 1983. Intercomparison of stable isotope reference samples. Nature 302, 236–238.
Coudé-Gaussen, G., Hillaire-Marcel, C., Rognon, P., 1982. Origine et évolution pédologique des fractions carbonatées dans les loess des Matmata (Sud-Tunisien) d'après leurs teneurs en 13C et 18O. CR Acad. Sci. Paris 295, 939–942.
Dasch, E.J., 1969. Strontium isotopes in profiles, deep-sea sediments, and sedimentary rocks. Geochim. Cosmochim. Acta 33, 1521–1552.
De Lange, G.J., Krijgsman, W., 2010. Messinian Salinity Crisis: a novel unifying shallow gypsum/ deep dolomite formation mechanism. Mar. Geol. 275, 273–277.
deMenocal, P.B., 1995a. Plio-Pleistocene African climate. Science 270–5233, 53–59.
deMenocal, P.B., 1995b. Plio-Pleistocene African climate. Science 270, 53–59.
deMenocal, P.B., 2004. African climate change and faunal evolution during the Pliocene–Pleistocene. Earth Planet. Sci. Lett. (Front.) 220 (1/2), 3–24.
deMenocal, P.B., Ruddiman, W.F., Pokras, E.M., 1993. Influences of high and low-latitude processes on African terrestrial climate: Pleistocene eolian records from equatorial Atlantic ocean drilling program Site 663. Paleoceanography 8–2, 209–242.
Duggen, S., Hoernie, K., van den Bogaard, P., Rupke, L., Phipps Morgan, J., 2003. Deep roots of the Messinian salinity crisis. Nature 422, 602–605.
Fauquette, S., Suc, J.-P., Bertini, A., Popescu, S.-M., Warny, S., Taoufiq, N.B., Villa, M.-J.P., Chikhi, H., Feddi, N., Subally, D., Clauzon, G., Ferrier, J., 2006. How much did climate force the Messinian salinity crisis? Quantified climatic conditions from pollen records in the Mediterranean region. Palaeogeogr. Palaeoclimatol. Palaeoecol. 238, 281–301.
Formenti, P., Schutz, L., Balkanski, Y., Desboeufs, K., Ebert, M., Kandler, K., Petzold, A., Scheuvens, D., Weinbruch, S., Zhang, D., 2011. Recent progress in understanding physical and chemical properties of African and Asian mineral dust. Atmos. Chem. Phys. 11, 8231–8256.
Gaillardet, J., Dupré, B., Allègre, C.J., 1999. Geochemistry of large river suspended sediments: silicate weathering or recycling tracer? Geochim. Cosmochim. Acta 63 (23–24), 4037–4051.
Garcia-Castellanos, D., Estrada, F., Jimenez-Munt, I., Gorini, C., Fernandez, M., Vergés, J., De Vicente, R., 2009. Catastrophic flood of the Mediterranean after the Messinian salinity crisis. Nature 462, 778–781.
Gargani, J., Rigollet, C., 2007. Mediterranean Sea level variations during the Messinian salinity crisis. Geophys. Res. Lett. 34, L10405. http://dx.doi.org/10.1029/2007/GL029885.
Gargani, J., Moretti, I., Letouzey, J., 2008. Evaporite accumulation during the Messinian Salinity Crisis: the Suez Rift case. Geophys. Res. Lett. 35, 1–6.
Gargani, J., Rigollet, C., Scarselli, S., 2010. Isostatic response and geomorphological evolution of the Nile valley during the Messinian salinity crisis. Bull. Soc. Geol. Fr. 181, 19–26.
Gasse, F., 2000. Hydrological changes in the African tropics since the Last Glacial Maximum. Quat. Sci. Rev. 19, 189–211.
Gautier, F., Clauzon, G., Suc, J.-P., Cravatte, J., Violanti, D., 1994. Age et durée de la crise de salinité messinienne. C. R. Geosci. 318, 1103–1109.
Gladstone, R., Flecker, R., Valdes, P., Lunt, D., Markwick, P., 2007. The Mediterranean hydrologic budget from a Late Miocene global climate simulation. Palaeogeogr. Palaeoclimatol. Palaeoecol. 251, 254–267.
Goudie, A.S., Middleton, N.J., 2001. Saharan dust storms: nature and consequences. Earth Sci. Rev. 56 (1–4), 179–204.
Govin, A., Holzwarth, U., Heslop, D., Keeling, L.F., Zabel, M., Mulitza, S., Collins, J.A., Chiessi, C.M., 2012. Distribution of major elements in Atlantic surface sediments (36°N–49°S): imprint of terrigenous input and continental weathering. Geochem. Geophys. Geosyst. 13. http://dx.doi.org/10.1029/2011GC003785 (23 PP.).
Griffin, D.L., 1999. The late Miocene climate of northeastern Africa: unravelling the signals in the sedimentary succession. J. Geol. Soc. 156, 817–826.
Griffin, D.L., 2002. Aridity and humidity: two aspects of the late Miocene climate of North Africa and the Mediterranean. Palaeogeogr. Palaeoclimatol. Palaeoecol. 182, 65–91.
Grousset, F.E., Biscaye, P.E., 2005. Tracing dust sources and transport patterns using Sr, Nd and Pb isotopes. Chem. Geol. 222, 149–167. http://dx.doi.org/10.1016/j.chemgeo.2005.05.006.
Grousset, F.E., Rognon, P., Coudé-Gaussen, G., Pedemay, P., 1992. Origins of Peri-Saharan dust deposits traced by their Nd and Sr isotopic composition. Palaeogeogr. Palaeoclimatol. Palaeoecol. 93 (3–4), 203–212.
Grousset, F.E., Parra, M., Bory, A., Martinez, P., Bertrand, P., Shimmield, G., Ellam, R.M., 1998. Saharan wind regimes traced by the Sr–Nd isotopic composition of subtropical Atlantic sediments: last Glacial Maximum vs today. Quat. Sci. Rev. 17, 395–409.
Hodell, D.A., Jason, H.C., Sierro, F.J., Raymo, M.E., 2001. Correlation of late Miocene to early Pliocene sequences between the Mediterranean and North Atlantic. Paleoceanography 16–2, 164–178.
Hsü, K.J., Cita, M.B., Ryan, W.B.F., 1973. The origin of the Mediterranean evaporites. Initial Rep. Deep Sea Drill. Proj. 13, 1203–1231.
Jones, A., Kaiteris, P., 1983. A vacuum gasometic technique for rapid and precise analysis of calcium carbonate in sediments and soils. J. Sediment. Petrol. 53, 655–660.
Kido, Y., Koshikawa, T., Tada, R., 2006. Rapid and quantitative major element analysis method for wet fine-grained sediments using an XRF microscanner. Mar. Geol. 229, 209–225.
Krijgsman, W., 2002. The Mediterranean: Mare Nostrum of Earth Sciences. Earth Planet. Sci. Lett. 205, 1–12.
Krijgsman, W., Hilgen, F.J., Raffi, L., Sierro, F.J., Wilson, D.S., 1999a. Chronology, causes and progression of the Messinian salinity crisis. Nature 400, 652–655.
Krijgsman, W., Hilgen, F.J., Marabini, S., Vai, G.B., 1999b. New paleomagnetic and cyclostratigraphic age constraints on the Messinian of the Northern Apennines (Vena del Gesso Basin, Italy). Mem. Soc. Geol. Ital. 54, 25–33.
Laskar, J., Robutel, P., Joutel, F., Gastineau, M., Correia, A.C.M., Levrard, B., 2004. A long term numerical solution for the insolation quantities of the Earth. Astron. Astrophys. 428, 261–285.
Liu, Z., Colin, C., Trentesaux, A., Blamart, D., Bassinot, F., Siani, G., Sicre, M.-S., 2004. Erosional history of the eastern Tibetan Plateau over the past 190 kyr: clay mineralogical and geochemical investigations from the southwestern South China Sea. Mar. Geol. 209, 1–18.
Lofi, J., Gorini, C., Berné, S., Clauzon, G., Dos Reis, A.T., Ryan, B.F., Steckler, M.S., 2005. Erosional processes and paleo-environmental changes in the Western Gulf of Lions (SW France) during the Messinian Salinity Crisis. Mar. Geol. 217, 1–30.
Loget, N., Van Den Driessche, J., Davy, P., 2005. How did the Messinian Salinity Crisis end? Terra Nova 17, 414–419.
Maillard, A., Gorini, C., Mauffret, A., Sage, F., Lofi, J., Gaullier, V., 2006. Offshore evidence of polyphase erosion in the Valencia Basin (Northwestern Mediterranean): scenario for the Mesiinian Salinity Crisis. Sediment. Geol. 188–189, 69–91.
Martin, J.-M., Meybeck, M., 1979. Elemental mass-balance of material carried by major world rivers. Mar. Chem. 7 (3), 173–206.
Meyer, I., Davies, G.R., Stuut, J.-B., 2011. Grain size control on Sr–Nd isotope provenance studies and impact on paleoclimate reconstructions: an example from deep-sea sediments offshore NW Africa. Geochem. Geophys. Geosyst. 12. http://dx.doi.org/10.1029/2010GC003355.
Molinaroli, E., 1996. Mineralogical characterization of Saharan dust with a view to its final destination in Mediterranean sediments. In: Guerzoni, S., Chester, R. (Eds.), The Impact of Desert Dust across the Mediterranean. Kluwer Academic, Dordrecht, pp. 153–162.
Murphy, L.N., Kirk-Davidoff, D.B., Mahowald, N., Otto-Bliesner, B.L., 2009. A numerical study of the climate response to lowered Mediterranean Sea level during the Messinian Salinity Crisis. Palaeogeogr. Palaeoclimatol. Palaeoecol. 279, 41–59.
Nesbitt, H.W., Young, G.M., 1982. Early Proterozoic climates and plate motions inferred from major element chemistry of lutites. Nature 299, 715–717.
Paillard, D., Labeyrie, L., Yiou, P., 1996. Macintosh program performs time-series analysis. EOS Trans. Am. Geophys. Union 77, 379.
Paillou, P., Schuster, M., Tooth, S., Farr, T., Rosenqvist, A., Lopez, S., Malezieux, J.-M., 2009. Mapping of a major paleodrainage system in eastern Libya using orbital imaging radar: The Kufrah River. Earth Planet. Sci. Lett. 277, 327–333.
Paquet, H., Coudé-Gaussen, G., Rognon, P., 1984. Étude minéralogique de poussières le long d'un itinéraire entre 19° et 35° de latitude nord. Rev. Géol. Dynam. Géog. Phys. 25, 257–265.
Pastouret, L., Chamley, H., Delibrias, G., Duplessy, J.C., Thiede, J., 1978. Late Quaternary climatic changes in western tropical Africa deduced from deep-sea sedimentation of the Niger delta. Oceanol. Acta 1, 217–232.
Petschick, R., 2000. MacDiff 4.2.2 [Online]. Available http://servermac.geologie.uni-frankfurt.de/Rainer.html (Cited 01-12-2001).
Prospero, M.J., Carlson, T.N., 1981. Saharan air outbreaks over the tropical North Atlantic. Pure Appl. Geophys. 119, 677–691.
Prospero, J.M., Nees, R.T., 1986. Impact of the North African drought and El Nino on mineral dust in the Barbados trade winds. Nature 320, 735–738.
Pye, K., 1989. Processes of fine particle formation, dust source regions, and climatic changes. In: Leinen, M., Sarnthein, M. (Eds.), Paleoclimatology and Palcometeorology: Modern and Past Patterns of Global Atmospheric Transport. Kluwer Academic, Norwell, MA, pp. 3–30.
Raffi, I., Backman, J., Fornaciari, E., Pälike, H., Rio, D., Lourens, L., Hilgen, F.J., 2006. A review of calcareous nannofossil astrobiochronology encompassing the past 25 million years. Quat. Sci. Rev. 25, 3113–3137.
Ratmeyer, V., Fischer, G., Wefer, G., 1999. Lithogenic particle fluxes and grain size distributions in the deep ocean off northwest Africa: implications for seasonal changes of aeolian dust input and downward transport. Deep-Sea Res. 46, 1289–1337.
Rea, D.K., 1994. The paleoclimatic record provided by eolian deposition in the deep sea: the geologic history of wind. Rev. Geophys. 32, 159–195.
Richter, T.O., Van der Gaast, S.J., Koster, B., Vaars, A., Gieles, R., de Stigter, H.C., de Haas, H., van Weering, T.C.E., 2006. The Avaatech XRF Core Scanner: technical description and applications to NE Atlantic sediments. In: Rothwell, G. (Ed.), New Ways of Looking at Sediment Cores and Core Data. Geol. Soc. Spec. Publ.
Riding, R., Braga, J.C., Martín, J.M., Sánchez-Almazo, I.M., 1998. Mediterranean Messinian Salinity Crisis: constraints from a coeval marginal basin, Sorbas, southeastern Spain. Mar. Geol. 146, 1–20.
Rouchy, J.M., Caruso, A., 2006. The Messinian salinity crisis in the Mediterranean Basin: a reassessment of the data and a integrated scenario. Sediment. Geol. 188–189, 35–67.
Ruddiman, W.F., Janecek, T.R., 1989. Pliocene–Pleistocene biogenic and terrigenous fluxes at equatorial Atlantic Sites 662, 663 and 664. Proc. ODP Sci. Results 108, 211–240.

Ruddiman, W.F., McIntyre, A., Raymo, M.E., 1986. Paleoenvironmental results from North Atlantic Sites 607–609. In: Ruddiman, W.F., et al. (Eds.), Init. Rep. Deep Sea Drilling Proj., 94, pp. 855–878.
Scheuvens, D., Schütz, L., Kandler, K., Ebert, M., Weinbruch, S., 2013. Bulk composition of northern African dust and its source sediments — a compilation. Earth Sci. Rev. 116, 170–194.
Schneck, R., Micheels, A., Mosbrugger, V., 2010. Climate modelling sensitivity experiments for the Messinian Salinity Crisis. Palaeogeogr. Palaeoclimatol. Palaeoecol. 286, 149–163.
Shackleton, N.J., Crowhurst, S., 1997. Sediment fluxes based on an orbitally tuned time scale 5 Ma to 14 Ma, Site 926. ODP Proc. 154, 69–82.
Shackleton, N.J., Hall, M.A., Pate, D., 1995. Pliocene stable isotope stratigraphy of Site 846. ODP Proc. 138, 337–355.
Skonieczny, C., Bory, A., Bout-Roumazeilles, V., Abouchami, W., Galer, S.J.G., Crosta, X., Stuut, J.-B., Meyer, I., Chiapello, I., Podvin, T., Chatenet, B., Diallo, A., Ndiaye, T., 2011. The 7–13 March 2006 major Saharan outbreak: Multiproxy characterization of mineral dust deposited on the West African margin. J. Geophys. Res. 116, D18210. http://dx.doi.org/10.1029/2011JD016173.
Skonieczny, C., Bory, A., Bout-Roumazeilles, V., Abouchami, W., Galer, S.J.G., Crosta, X., Diallo, A., Ndiaye, T.A., 2013. Three-year time series of mineral dust deposits on the West African margin: sedimentological and geochemical signatures and implications for interpretation of marine paleo-dust records. Earth Planet. Sci. Lett. 364, 145–156.
Stein, R., Sarnthein, M., 1984. Late Neogene oxygen isotope stratigraphy and terrigenous flux rates at Site 544B off Morocco. Init. Rep. Deep Sea Drilling Proj. 79, 385–394.
Stuut, J.-B., Zabel, M., Ratmeyer, V., Helmke, P., 2005. Provenance of present-day eolian dust collected off NW Africa. J. Geophys. Res. 110, 1–14.
Swap, R., Garstang, M., Macko, S.A., 1996. The long-range transport of southern African aerosols to the tropical South Atlantic. J. Geophys. Res. 101, 23,777–23,791.
Tiedemann, R., Sarnthein, M., Stem, R., 1989. Climatic changes in the western Sahara: aeolo-marine sediment record of the last 8 million years (Sites 657–661). Proc. ODP Sci. Results, 108, pp. 241–261.
Tiedemann, R., Sarnthein, M., Shackleton, N.J., 1994. Astronomic timescale for the Pliocene Atlantic d18O and dust flux records of Ocean Drilling Program Site 659. Paleoceanography 9 (4), 619–638.
Tjallingii, R., Röhl, U., Kölling, M., Bickert, T., 2007. Influence of the water content on X-ray fluorescence core-scanning measurements in soft marine sediments. Geochem. Geophys. Geosyst. 8, Q02004. http://dx.doi.org/10.1029/2006GC001393.
Topper, R.P.M., Meijer, P.T.H., 2013. A modelling perspective on spatial and temporal variations in Messinian evaporite deposits. Mar. Geol. 336, 44–60.
Tuenter, E., Weber, S.L., Hilgen, F.J., Lourens, L.J., 2003. The response of the African summer monsoon to remote and local forcing due to precession and obliquity. Glob. Planet. Chang. 36, 219–235.
Vidal, L., Bickert, T., Wefer, G., Rohl, U., 2002. Late Miocene stable isotope stratigraphy of SE Atlantic ODP Site 1085: Relation to Messinian events. Marine Geology 180, 71–85.
Vörösmarty, C.J., Fekete, B.M., Meybeck, M., Lammers, R.B., 2000. Global system of rivers: its role in organizing continental land mass and defining land-to-ocean linkages. Glob. Biogeochem. Cycles 14 (2), 599–621.
Warny, S.A., Bart, P.J., Suc, J.-P., 2003. Timing and progression of climatic, tectonic and glacioeustatic influences on the Messinian salinity crisis. Palaeogeogr. Palaeoclimatol. Palaeoecol. 202, 59–66.
Watkins, D.K., Bergen, J.A., 2003. Late Albian adaptive radiation in the calcareous nannofossil genus Effellithus. Micropaleontology 49, 231–252.
Weeks, R., Laj, C., Endignoux, L., Fuller, M., Roberts, A., Manganne, R., Blanchard, E., Goree, W., 1993. Improvements in long-core measurement techniques: applications in palaeomagnetism and palaeoceanography. Geophys. J. Int. 114, 651–662.
Wehausen, R., Brumsack, H.J., 1999. Cyclic variations in the chemical composition of eastern Mediterranean Pliocene sediments: a key for understanding sapropel formation. Mar. Geol. 153, 161–176.
Wilke, B.M., Duke, B.J., Jimoh, W.L.O., 1984. Mineralogy and chemistry of Harmattan dust in northern Nigeria. Catena 11, 91–96.
Willett, S.D., Schunegger, F., Pizotti, V., 2006. Messinian climate change and erosional destruction of the central European Alps. Geology 34, 613–616.
Wynn, R.B., Masson, D.G., Stow, D.A.V., Weaver, P.P.E., 2000. The Northwest African slope apron: a modern analogue for deep-water systems with complex seafloor topography. Mar. Pet. Geol. 17, 253–265.
Zhao, Y., Colin, C., Liu, Z., Paterne, M., Siani, G., Xie, X., 2012. Reconstructing precipitation changes in the northeastern Africa during the Quaternary by clay mineralogical and geochemical investigation of Nile deep-sea fan sediments. Quat. Sci. Rev. 57, 58–74.